5-2021

Investigation of the C—CN Bond Activation of Fluorinated Benzonitriles with [Ni(dmpe)] and Dft Benchmarking Study with [Ni(dippe)]

Dominique C. Gallegos
The University of Texas Rio Grande Valley

INVESTIGATION OF THE C—CN BOND ACTIVATION OF FLUORINATED BENZONITRILES WITH [Ni(dmpe)] AND DFT BENCHMARKING STUDY WITH [Ni(dippe)]

A Thesis

by

DOMINIQUE C. GALLEGOS

Submitted to the Graduate College of
The University of Texas Rio Grande Valley
In partial fulfillment of the requirements for the degree of

MASTER OF SCIENCE

May 2021

Major Subject: Chemistry

INVESTIGATION OF THE C—CN BOND ACTIVATION OF FLUORINATED BENZONITRILES WITH [Ni(dmpe)] AND DFT BENCHMARKING STUDY WITH [Ni(dippe)]

A Thesis
by
DOMINIQUE C. GALLEGOS

COMMITTEE MEMBERS

Dr. Tülay A. Ateşin
Chair of Committee

Dr. William D. Jones
Committee Member

Dr. Shervin Fatehi
Committee Member

Dr. Debasish Bandyopadhyay
Committee Member

May 2021

ABSTRACT

Gallegos, Dominique C., Investigation of the C—CN Bond Activation of Fluorinated Benzonitriles with [Ni(dmpe)] and DFT Benchmarking Study with [Ni(dippe)]. Master of Science (MS), May, 2021, 68 pp., 10 tables, 24 figures, 73 references, 27 titles.

Carbon-carbon bond activation has become a rapidly growing area of research due to its extensive range of applications. Despite the significant progress that has been made in this field, the cleavage of kinetically inert and thermodynamically stable C—C σ-bonds under mild homogeneous conditions remains a challenge. The activation is primarily limited to systems in which either relief of strain or aromatization serves as a driving force. A notable exception to this is the oxidative addition of unstrained C—CN bonds of nitriles. In this study, we are looking at the effect of fluoro substituents. We hypothesized that the number of *ortho*-F substituents would affect the product stability, rather than the total number of fluoro substituents. The benzonitrile substrates investigated are the 2-F, 3-F, 4-F, 2,6-F_2, and 3,5-F_2benzonitriles. The effects on the C—CN bond activation reaction of the fluorinated benzonitriles were investigated using [Ni(dmpe)] as a model for [Ni(dippe)] with DFT calculations. Both experimental and DFT calculation results have shown that there is a very good correlation between the stability of the C—CN bond activation products and the number of *o*-fluoro substituents. Although the C—C bond activation barrier is relatively constant with a slightly higher barrier for 2,6-F_2 substrate due to steric hindrance, the activation barriers for the C—C bond elimination show a good correlation with the number of *o*-F substituents. For the future work, we will continue the DFT analysis with [Ni(dippe)] using the results from our benchmarking study.

DEDICATION

With the unconditional love and emotional support of my family and friends, I dedicate this thesis and all my academic achievements to you all. Thanks to you, I have reached a new milestone in my life. First, I dedicate this work to my best friend, Zoe. I consider you a sister. Thank you for your friendship, acceptance, and all those special moments when we laugh uncontrollably remembering our crazy adventures and while watching our favorite movies. I deeply thank my husband, Ruben, who has been there by my side since I was an undergraduate at UT Austin. I do not know how you put up with me some days, but I am very grateful. I would also like to thank my husband's family: Alejandra, Alejandro, Elisa and Ruben. Gracias por bien venirme a la familia. And the ones who are not here anymore, it pains me that you cannot enjoy this moment with me, but I know that you are proud of me wherever you are. To my brother and his wife: Nick and Anna. Thank you for letting me be me around you and for being there to talk about anything. To my sister and her husband: Lisa and Hugo. Thank you for supporting me and for being the most enjoyable people to be around. To my oldest sister and her husband: Angela and Roli. I hope I have become the respectable adult you both wanted me to become and I deeply appreciate your guidance and work ethic. And finally, I dedicate all my work to my parents: Sylvia and Raul. I would not be here without you. Thank you for pushing me to always do my best and for continuously believing in me. I cannot put into words the love and gratitude I feel for you.

ACKNOWLEDGEMENTS

I would first like to thank my research advisor and thesis committee chair Dr. Tülay Ateşin for all her mentoring and patience that she has had working with me these past two years. As my academic mother, she has invested so much time in teaching me everything I needed to know, and I aspire to be a remarkable chemist like her. I would also like to thank Dr. Abdurrahman Ateşin who was more than generous with his expertise and time. I wish to thank my committee members, Dr. Jones, Dr. Fatehi, and Dr. Bandyopadhyay "Dr. Deb." Dr. Jones, your guidance has helped me grow so much as a chemist. It has been a great honor and privilege to have worked with you. Dr. Fatehi, you were always there for me whenever I needed advice and I would like to thank you for always encouraging me. Dr. Deb, I always enjoy your company and I appreciate your willingness to help. I would also like to thank my colleagues Lubna Kader, Juliana Rodriguez, and Orion Nguyen. Your assistance throughout this research was more than valuable. Finally, I would like to thank the University of Texas at Rio Grande Valley and the Chemistry Department which made the completion of this degree an enjoyable experience.

TABLE OF CONTENTS

Page

ABSTRACT ……. iii

DEDICATION ……. iv

ACNOWLEDGEMENTS …… v

TABLE OF CONTENTS ……. vi

LIST OF TABLES ……... viii

LIST OF FIGURES ……..…. x

CHAPTER I. INTRODUCTION ……. 1

C-C Activation ……..……. 1

CHAPTER II. BACKGROUND …….. 4

C-CN Activation …… 4

Nickel ……... 5

CHAPTER III. METHODOLOGY …….. 11

Density Functional Theory (DFT) …… 11

Foundations of DFT ……. 12

Functional Taxonomy and Exchange-Correlation Functionals …… 15

Dispersion Interactions in DFT …… 21

Which Functional Should You Choose? …….. 22

Computational Details …….. 22

CHAPTER IV. RESULTS AND DISCUSSION ……. 24

Interatomic Distances and Bond Angle Analysis ……. 24

Predicted *o*-Fluorine Effect …… 28

Energy Analysis ……..... 30

DFT Benchmark Analysis ……. 35

Future Work ……... 53

CHAPTER V. CONCLUSIONS ……... 54

REFERENCES …….. 55

BIOGRAPHICAL SKETCH ……. 68

LIST OF TABLES

Page

Table 1: Selected Interatomic Distances (in Å) for η2-CNs Involved in C—C Bond Activation calculated by using Gaussian16, B3LYP/C, H, N, F (6-31G**), Ni, P (SDDALL) α_{Ni} = 3.130, α_P = 0.387/SMD (toluene/THF) …… 25

Table 2: Selected Interatomic Distances (in Å) for OA products calculated by Gaussian16, B3LYP/C, H, N, F (6-31G**), Ni, P (SDDALL) α_{Ni} = 3.130, α_P = 0.387/SMD (toluene/THF) ……. 26

Table 3: Selected Interatomic Distances (in Å) for TSs Involving in C−C Bond Activation calculated by Gaussian16, B3LYP/C, H, N, F (6-31G**), Ni, P (SDDALL) α_{Ni} = 3.130, α_P = 0.387/SMD (toluene/THF) ……. 28

Table 4: A comparison of the experimental ΔG values obtained from the Van't Hoff plots and the calculated ΔG values with [Ni(dmpe)] by using Gaussian16/ B3LYP/C, H (6-31G**); Ni, P (SDDALL) α_{Ni} = 3.130, α_P = 0.387/SMD (toluene/THF) …. 30

Table 5: DFT Calculations with [Ni(dmpe)] Complexes. Energies are in kcal/mol and calculated by using Gaussian16, B3LYP/C, H, N, F (6-31G**), Ni, P (SDDALL) α_{Ni} = 3.130, α_P = 0.387/SMD (toluene/THF) …… 31

Table 6: Functionals that were used for full ligand DFT calculations and their reported energies. ΔG is reported in kcal/mol calculated by using Gaussian16/C, H (6-31G**); Ni, P (SDDALL), α_{Ni} = 3.130, α_P = 0.387/SMD (toluene/THF) … 36

Table 7: Table energetics, zero-point energy calculations, enthalpy, entropy, and thermal corrections for each DFT method …….. 39

Table 8: Experimental and Expected ΔG values of Benzonitrile Nickel Complexes in THF and Toluene with correction …….. 45

Table 9: Solvation Energies and Thermochemical Corrections for C—CN Bond Activation of Fluorinated Benzonitriles …….. 51

Table 10: ΔG Calculated for C—CN Bond Activation of Fluorinated Benzonitriles …… 52

LIST OF FIGURES

Page

Figure 1: Comparison of the interactions of metal orbitals with C—C and C—H s bonds …. 2

Figure 2: Two common pathways for C—CN bond activation ……..... 4

Figure 3: Silicon-assisted C—CN bond activation mechanism ……... 5

Figure 4: Iron-assisted C—CN bond activation mechanism ……..... 5

Figure 5: General 3-step adiponitrile (AdN) synthesis ……..... 6

Figure 6: Proposed mechanism for isomerization ……..... 7

Figure 7: C—C bond activation with Ni using aryl nitriles …… 8

Figure 8: C—C bond activation with Ni using alkyl nitriles ……. 8

Figure 9: C—C bond activation with Ni using allyl nitriles …….……. 9

Figure 10: Jones' group obtained mostly linear product by using a similar process employing different solvents at different temperatures ……..…… 9

Figure 11: C—C bond activation with Ni using 2CN thiophene ……..... 10

Figure 12: Lewis acid assisted C—C bond activation with Ni …….. 10

Figure 13: Comparison of the interactions of metal orbitals with C—C and C—H s bonds …. 10

Figure 14: Depiction of Jacob's Ladder with the functionals that was used for the full ligand [Ni(dippe)] DFT calculations ……. 16

Figure 15: η^2-nitrile complex of [Ni(dmpe)] with 2,6-difluorobenzonitrile …… 25

Figure 16: C—C bond activation product of the reaction of [Ni(dmpe)] with 2,6-difluorobenzonitrile …… 26

Figure 17: Transition state structure for the C—C bond activation of 2,6-difluorobenzonitrile with [Ni(dmpe)] ……. 28

Figure 18: Predicted *o*-Fluorine Effect on Calculated ΔG Values by using Gaussian16, B3LYP/C, H, N, F (6-31G**), Ni, P (SDDALL) α_{Ni} = 3.130, α_P = 0.387/SMD (toluene/THF) …… 29

Figure 19: Predicted *o*-Fluorine Effect on Calculated $\Delta G^{\ddagger}$ (RE) Values by using Gaussian16, B3LYP/C, H, N, F (6-31G**), Ni, P (SDDALL) α_{Ni} = 3.130, α_P = 0.387/SMD (toluene/THF) …… 29

Figure 20: ΔG (kcal/mol) calculated for the C—CN bond activation reaction by using Gaussian16, B3LYP/C, H, N, F (6-31G**), Ni, P (SDDALL) α_{Ni} = 3.130, α_P = 0.387/SMD (toluene/THF) …… 32

Figure 21: $\Delta G^{\ddagger}$ (kcal/mol) calculated for the C—CN bond activation reaction by using Gaussian16, B3LYP/C, H, N, F (6-31G**), Ni, P (SDDALL) α_{Ni} = 3.130, α_P = 0.387/SMD (toluene/THF) …….. 33

Figure 22: $\Delta G^{\ddagger}$ (kcal/mol) calculated for the C—CN reductive elimination by using Gaussian16, B3LYP/C, H, N, F (6-31G**), Ni, P (SDDALL) α_{Ni} = 3.130, α_P = 0.387/SMD (toluene/THF) …….. 34

Figure 23: C—H aryl interactions observed in the [Ni(dippe)] ligand …… 37

Figure 24: Variation of the isopropyl group orientations observed in the [Ni(dippe)] ligand. These are also the two most stable [Ni(dippe)] conformers …….. 37

CHAPTER I

INTRODUCTION

C–C Bond Activation

In recent years, there has been a significant increase in research involving the activation of carbon-carbon (C–C) bonds. It is widely accepted that C–C bond formation is fundamental to organic synthesis. Researchers have developed various ways to create C–C bonds, however reactions involving the cleavage of C–C bonds catalyzed by homogeneous transition-metal complexes are rare. Several key reactions that form C–C bond are cross-coupling, cycloaddition, alkylation, and aldol reactions. C–C bond cleavage reactions, such as retro Diels-Alder, Cope and Claisen rearrangements, and ozonolysis of alkenes have found extensive applications in complex molecule synthesis. The overall goal of current C–C bond activation is converting relatively simple compounds into more complex products. It is important to note that two or more new C–C (or C–X) bonds may form by breaking one C–C bond. In general, cleaving C–C bonds is not a destructive process and it provides opportunities for researchers to develop novel transformations through employing such distinct modes of reactivity.

Although the activation of C–C bonds has many potentially important applications both in industrial processes and organic synthesis, the insertion of a transition metal into a C–C bond is difficult to achieve due to the inertness of C–C σ bonds.[1] The lack of reactivity behind these bonds can be attributed to their thermodynamic stability and kinetic inaccessibility. It has proven to be a challenge to break a more stable C–C bond to form two less stable M–C bonds. A common strategy used to contest this is the relief of ring strain.[2] In organometallic chemistry, the

kinetic inaccessibility behind C–C bonds can be attributed to the directionality of its σ orbital as well as the substituents located on one or both carbons. These make it harder for a metal to insert into a C–C bond. In comparison, C–H bonds are sterically more accessible and easier to activate. In most cases, C–H bond activation is observed prior to C–C bond activation. Figure 1 shows a comparison of the competing interactions of metal orbitals with C–C and C–H single bonds:

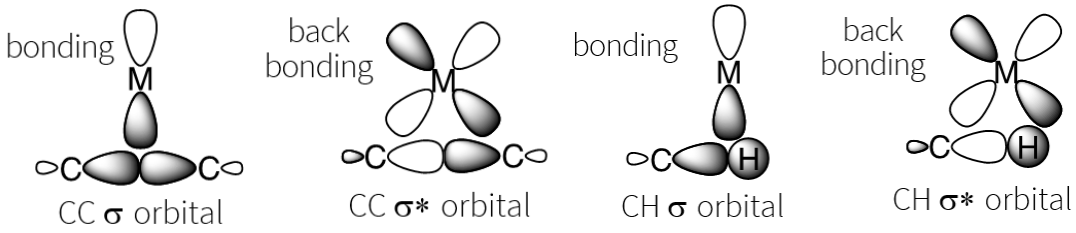

Figure 1: Comparison of the interactions of metal orbitals with C—C and C—H σ bonds.

Both σ orbitals connecting the C,C and C,H atoms lie along the bond axis. The constituent 1s orbital of the H atom is spherical. It has no other substituents except the bonded C, making an end-on approach to a metal sterically viable. In fact, Crabtree et al. proposed that the route of oxidative addition of a C–H bond to a metal begins with an end-on approach prior to side-on coordination.[2] The interaction of directional and sterically strained C-C σ orbital with metal orbitals is much more difficult than that of a C–H σ bond. This kinetic barrier makes the C–C bond considerably inert. Thus, breaking C–C bonds by the insertion of transition metal complexes has been a challenging issue in the field of organometallic chemistry.

There are three categories that divide transition-metal catalyzed C-C bond activation reactions showcased in Scheme 1. The first main pathway is the C–C bond activation via oxidative addition (path A).[3] This is the reverse reaction pathway of the C–C bond formation through reductive elimination. In this instance, the metal is inserted into the C-C bond and the

oxidation state of the metal increases by two. A second pathway is the *β*-carbon elimination (path B) which is entropically driven.[4] This pathway is the carbon equivalent of the common β-hydride elimination reaction of organometallics. The configuration of a strong C═X bond (X = O) typically contributes to the driving force of this process. Additionally, in the case of strained cyclic substrates, a ring-strain release facilitates the C–C bond cleavage. For acyclic substrates, the formation of a stable byproduct generated from an entropy increase allows for the success of the reaction. Lastly, the third main pathway is the retro-allylation (path C) reaction. This mechanism proceeds via a six-membered transition state and produces an allyl metal species.[5]

Path A: Oxidative Addition

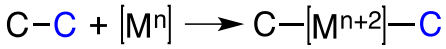

Path B: *β*-Carbon Elimination

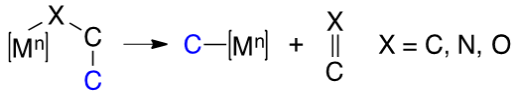

Path C: Retro-Allylation

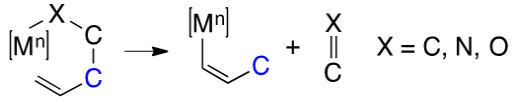

Scheme 1: The three categories involving transition-metal-catalyzed C–C bond activation.

Numerous methods have been recognized as favoring C–C cleavage with transition metal complexes. Common examples that contribute to C-C cleavage are the relief of ring strain, the attainment of aromaticity, and even proximity. Several systems where mechanistic information has been obtained in C-C cleavage include biphenylene, C-CN bonds, C-C≡C bonds, and aryl-CH_3 bonds. In the following chapter, we will solely examine the mechanistic studies behind the C-C cleavage of C-CN bonds.

CHAPTER II

BACKGROUND

C—CN Bond Activation

Due to the industrial importance of C—CN bond activation, the C—C bond activation of nitriles have been extensively studied. For example, the oxidative addition of C—CN bonds at low valent transition metals was recognized over 40 years ago. The reverse reaction, reduction elimination to form a C—CN bond, has also been recorded.

There are two pathways commonly accepted for the activation of C—CN bonds that are observed in Figure 2. The first step involves the coordination of the metal into the C—N bond, which may coordinate either through η^2 or η^1 from the N end. The pathway where rhodium and iron are listed is called the silicon-assisted mechanism shown in Figure 3. It was first reported by Brookhart that the silicon coordinates to the cyanide and activates it.[6] Nakazawa reported a similar pathway involving iron in showcased in Figure 4.[7]

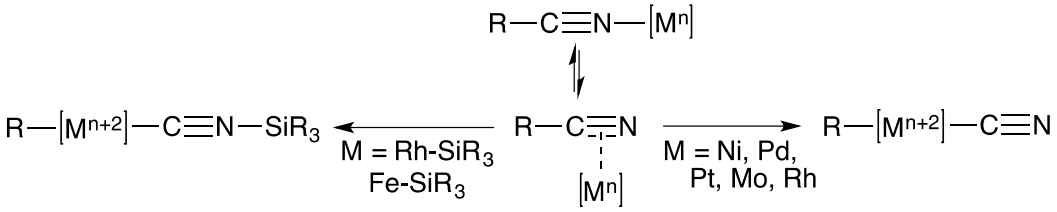

Figure 2: Two common pathways for C—CN bond activation.

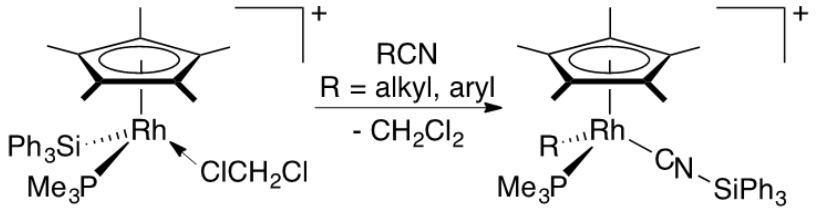

Figure 3: Silicon-assisted C—CN bond activation mechanism.

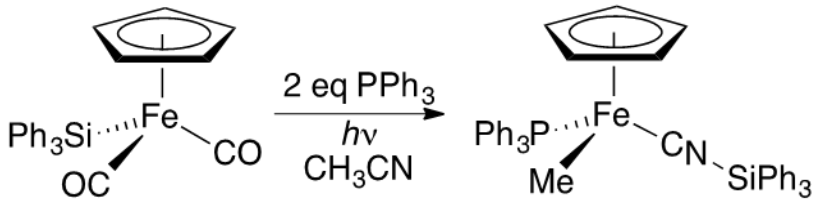

Figure 4: Iron-assisted C—CN bond activation mechanism.

Nickel

Despite the resurgence of interest to develop alternative nickel catalysts due to the cost of palladium and platinum, the organometallic chemistry of nickel is not well understood. The methods involving nickel are underdeveloped and face many challenges. In comparison to Pd, although Ni catalytic cycles follow the Ni(0)/Ni(II) pathway, odd oxidation states such as in Ni(I)/Ni(III) cycles are more readily accessible and involved in numerous Ni catalyzed transformations. The highest oxidation state of IV however is quite uncommon for Ni as opposed to Pd,[22] where numerous catalytic cycles involve Pd (IV) intermediates.[23-24]

A significant industrial process reported in 1971 that focuses on nickel insertion with C—CN cleavage is the hydrocyanation of butadiene to produce adiponitrile (AdN).[8] This involves a three-step process shown in Figure 5 where the hydrogenation of adiponitrile gives 1,6-diaminohexane, a coupling partner with adipic acid to produce nylon-6,6. In the DuPont

adiponitrile process, adiponitrile is produced by the addition of HCN across butadiene twice in anti-Markovnikov fashion. The issue here is that the first addition goes preferably to give the Markovnikov product which is branched rather than linear. The branched isomer is more stable; however, the linear product is sought after. The DuPont process includes a nickel-based catalyst that reversibly cleaves the C—CN bond, permitting for the branched isomer 2-methyl-3-butene nitrile to be balanced with the linear isomer 3-pentene nitrile (3PN). With a Lewis acid, isomerization produces 4-pentene nitrile (4PN) which is consumed in a second HCN addition to produce AdN.

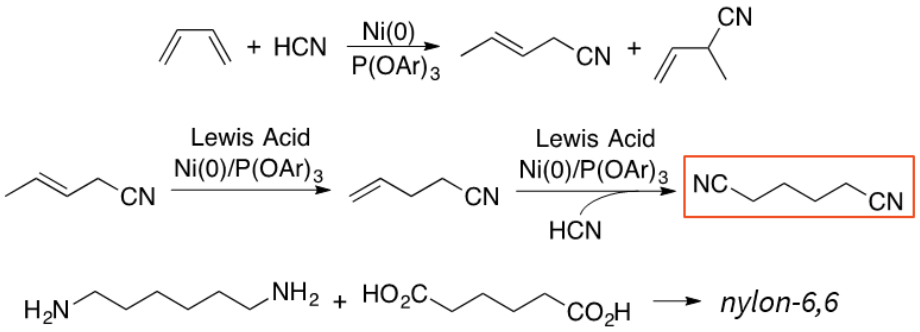

Figure 5: General 3-step adiponitrile (AdN) synthesis.

The key is to isomerize the unwanted branched isomer to obtain the favored linear isomer by moving the cyano group from one end of the allyl to the other. Early mechanistic studies on this catalysis were carried out using phosphite ligands on nickel. Researchers recorded evidence for HCN addition and diene insertion to produce π-allyl nickel cyanide complexes, which then underwent reductive elimination of both branched and linear nitrile. In Figure 6, the proposed mechanism for isomerization shows this competition between the C—H bond activation and the C—C bond activation.[9] Steric effects were believed to be critical in determining the obtained product.

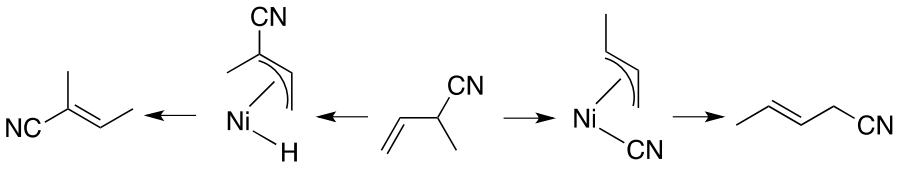

Figure 6: Proposed mechanism for isomerization.

Jones has reported extensively on how to activate C—CN bonds using nickel. In 2000, Jones' group first discovered an instance where C—CN cleavage was reversible. Using $[Ni(dippe)H]_2$ as a source of [Ni(dippe)] (dippe: bisdiisopropylphosphinoethane), a reaction with benzonitrile led initially to the formation of Ni(dippe)(η^2 -NCPh). After heating the nickel complex to 60°C for a few hours, conversion to the C—CN oxidative addition product Ni(dippe)(Ph)(CN) was observed. It was also later reported that the reaction did not reach completion and that indeed there was an equilibrium between these two nickel complexes.[10] In Figure 7, this reaction involving the aryl nitriles is shown. By changing the polarity of the solvent or by variation of the para-substituent on the phenyl group, the equilibrium position can be controlled.[11] A polar solvent, such as THF, was found to drive the equilibrium towards the more polar C—CN cleavage product, while a nonpolar solvent, such as toluene, drives the equilibrium towards the less polar η^2-nitrile complex. Density Functional Theory (DFT) calculations were conducted to further understand the mechanism of the C—CN cleavage. By replacing the dippe ligand with a simpler dmpe (bisdimethylphosphineoethane) ligand, DFT calculations proved that the reaction of acetonitrile with a zerovalent [Ni(dmpe)] fragment favors the initial η^2 coordination of the nitrile to Ni and gives the C—CN bond activation product exclusively under both thermal and photochemical conditions. Although the reaction of the $[Ni(dippe)H]_2$ complex with 2-methyl-2-butenenitrile provides evidence for the C—H bond activation, no C—H oxidative addition product was observed in the reaction with acetonitrile.[12]

These concepts were further extended to investigate ortho-, meta-, and para-dicyanobenzenes to give η^2-NCaryl and C—CN cleavage products.[13]

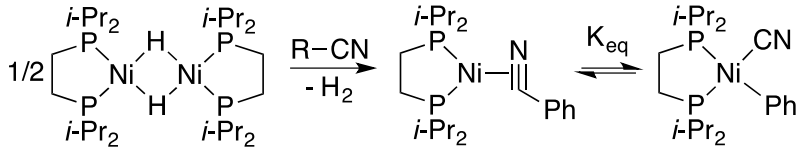

Figure 7: C—C bond activation with Ni using aryl nitriles

After the initial discovery of C—CN bond activation, Jones' group investigated the C—CN bond cleavage of alkyl nitriles with an identical nickel system shown in Figure 8. Similar to aryl nitriles, alkyl nitriles react to form π-complexes at room temperature. By heating the system, oxidative addition to the C—CN bond occurs which gives the methyl cyanide complex in the case of acetonitrile.[14] On the other hand, other alkyl derivatives undergo β-elimination to give the olefin, Ni(dippe)(η^2-olefin) and transient Ni(dippe)(H)(CN). The latter is unstable and decomposes to give Ni(dippe)$(CN)_2$. Unlike the aryl nitriles, the acetonitrile insertion reaches completion and does not appear to be reversible. DFT calculations confirmed that Ni(dippe)(CH_2CN)(H) undergoes reductive elimination at -40°C to give the π -complex.[15]

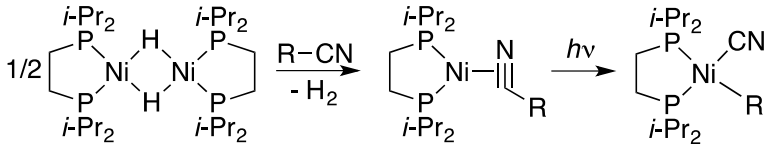

Figure 8: C—C bond activation with Ni using alkyl nitriles

Jones' work with the [Ni(dippe)] fragment incited the investigation of allyl nitriles as substrates for C—CN activation. It was observed that $[Ni(dippe)H]_2$ reacts with allylcyanide to

first produce an η^2-olefin complex, not a η^2-NC complex. This species then rearranges to give a π-allyl cyanide complex, a 5-coordinate square pyramidal structure with apical cyanide. The C—CN addition is reversible and over time, C–H activation occurs to isomerize the double bond into conjugation with the nitrile. C—CN cleavage was later observed exclusively to give the 5-coordinate square pyramidal product with BPh_3 attached to the cyanide ligand.[16] The general scheme using the allyl nitriles is observed in Figure 9. The [Ni(dippe)] fragment was also studied for its reactivity with 2-methyl-3-butenenitrile in stoichiometric experiments. Initial formation of the η^2 -alkene adduct (two isomers) leads to competitive C—H and C—CN activation. The π-allyl cyanide is observed, but the π-allyl hydride is not which is seen in Figure 10.[17] Extensive DFT calculations were made using dmpe as a model for dippe and revealed that the calculations agreed well with the experimental data and showed the preference of C—CN cleavage over C—H cleavage.[18]

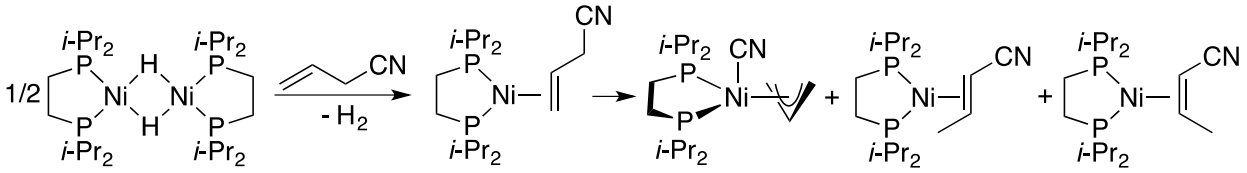

Figure 9: C—C bond activation with Ni using allyl nitriles

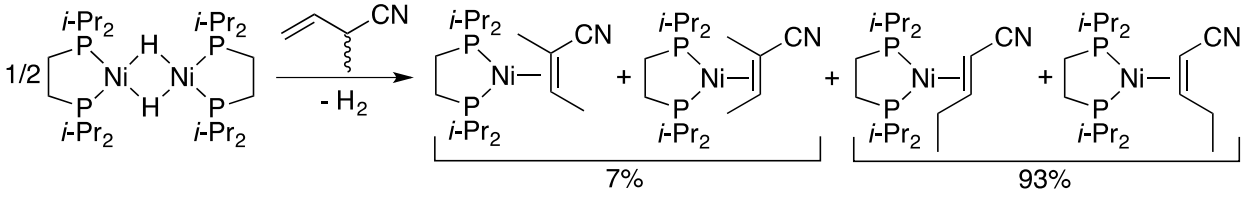

Figure 10: Jones' group obtained mostly linear product by using a similar process employing different solvents at different temperatures

Jones investigated several other systems to further document C—C bond activation with Ni. Further experiments included research involving 2-CN thiophene,[19] hemilabile ligands[20] and Lewis acids.[21] The processes for these reactions are seen in Figures 11-13.

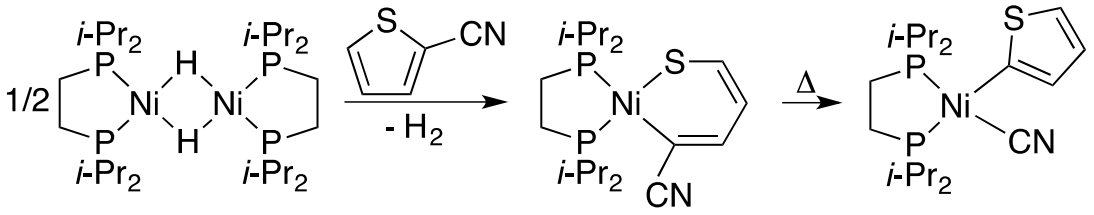

Figure 11: C-C bond activation with Ni using 2-CN thiophene

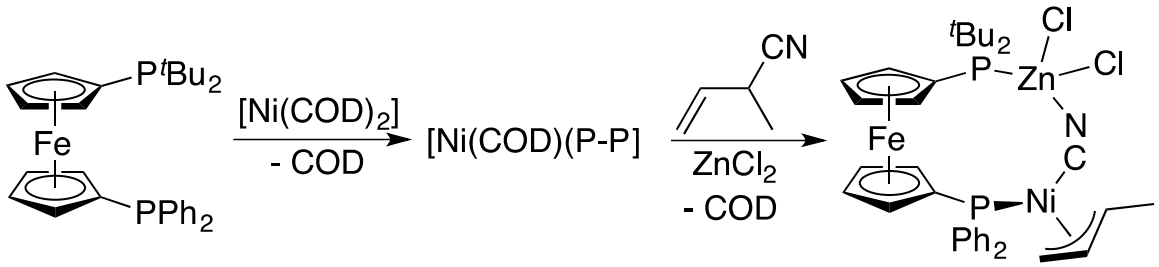

Figure 13: Lewis acid assisted C-C bond activation with Ni

CHAPTER III

METHODOLOGY

Density Functional Theory

In recent years, density functional theory (DFT) has become a standard method for analyzing bond energies, molecular structure, and reactivity in metallic compounds. Since initial development in the late 1980s and early 1990s, the number of DFT functionals has substantially increased due to the need for more cost efficient and accurate DFT methods.[32] Conducting a literature search reveals that over 20,000 papers were published in academic journals in 2020 with the words 'DFT' or 'B3LYP' (the most popular density functional) mentioned in the abstract.

Through the years, there has been constant development and need of more accurate density functionals. Although computational electronic structure methods are used in a straightforward and relatively inexpensive way to learn more about most systems, some problems remain that affect the accuracy of DFT. For instance, one issue is that common density functionals do not replicate pure dispersion interactions between unbound chemical species well. Another common issue is the poor cancellation between the electron self-interaction present in the Coulomb term and the exchange energy. As we will later discuss, this interaction does not completely cancel and there remains a residual self-interaction term that may lead to significant errors – a common example being the H_2^+ one-electron system.[60] Lastly, the third problem is that even the finest current exchange-correlation functionals can still lead to unacceptably large

energy errors for a significant number of 'outlier' species, even when dispersion and self-interaction are not involved.

Before looking into the density functionals used for this study, it is important to understand what DFT is and where it originates from.

Foundations of DFT

To solve the many-electron time-independent Schrödinger equation, one must employ the Born-Oppenheimer approximation in order to answer for the electronic degrees of freedom.[58] The idea from adding this approximation is to separate the motion of the nuclei and the motion of the electrons, by stating that the nuclei are stationary. The nuclei, however, can be stationary at different positions so the electronic wavefunction can depend on the positions of the nuclei even though their motion is neglected. Therefore, this approximation neglects the effect of the nuclear kinetic energy on the electrons. The fact that this assumption works can be traced to the fact that the nuclear masses are much larger than the electron mass. The electrons are assumed to respond to the motion of the ions, which generates a static external potential.

The Hartree-Fock (HF) method works to solve for the *N*-body Schrödinger equation by assuming that the many-electron wavefunction takes the form of a determinant of single-electron wavefunctions, called a Slater determinant. Since development, notable progress has been attained by using HF as a basis when calculating the ground state energy and creating the Random Phase Approximation (RPA) and the Random Phase Approximation with Exchange (RPAE) to investigate the dynamic properties of atoms and molecules.[61] Although widely used, HF method faces many problems in its application. For example, one requires a whole set of single-particle wave functions to calculate the single-electron nonlocal potential. With this

method, it is also necessary to follow a rather intricate procedure to incorporate the electronic correlation corrections that are past the HF basis and as a result, in the case of complex *N*-electron systems, the calculations become too complicated and the resulting energies tend to be too high.[35] DFT provides an appealing alternative as it provides a way to bypass the *N*-electron wavefunction in favor of the electron density.[35]

In 1964, Hohenberg and Kohn established the theorems which state that the total electron density completely and exactly determines all ground-state properties of an *N*-electron system and the ground-state energy can be obtained variationally.[33] The energy expression is typically written as eq. (1):

$$E[\rho] = \int v(r)\rho(r)dr + J(\rho) + T_S(\rho) + E_{XC}(\rho) \quad (1)$$

The $v(r)\rho(r)dr$ term represents the electromagnetic interaction of the electron density with the "external potential" which corresponds to the coulombic interactions between electrons and nuclei. The $J(\rho)$ term is the Coulomb energy and represents the repulsion between the electron density and itself. The $T_S(\rho)$ term approximates the electronic kinetic energy. The $E_{XC}(\rho)$ term is the exchange-correlation functional and this corrects the first three terms.

Though in practice, the Hohenberg-Kohn theorems did not prove to be very straightforward to complete orbital-free DFT calculations. Kohn and Sham proposed an alternative approach that extended on these ideas to overcome this problem. In the Kohn-Sham formulation, a fictitious system of non-interacting electrons is constructed in such a way that its exact ground-state density is the same as that of the interacting electrons.[36] By using this method, the calculation time is much shorter than that of a traditional direct approach, and so much larger complexes can be routinely handled.[38] The Kohn-Sham equations are the foundation of all recent

DFT applications and solving these equations leads in principle to the exact energy and density of the target system.

It is important to further describe that DFT functionals use a standard treatment of electron-electron interactions that effectively includes repulsion between an electron and itself. This self-interaction is partially corrected by the exchange part included in the functional. Currently, DFT computations allow for the modeling of full ligands without the need for molecular truncations, which is known to alter the steric and electronic properties of a system.[39] Although promising results have been reported for the performance of DFT in organometallic systems benchmarks,[25] standard DFT in some cases fails spectacularly. For example, an underestimation of absolute metal-ligand bond strengths of up to about 40 kcal/mol is seen with one of the popular functionals in the literature, B3LYP.[26-27] A part of this error can be recovered if empirical dispersion corrections are included such as those reported by Grimme et.al (D2,[28] D3,[29] or D3BJ[30]), which leads to DFT-D methods. Dispersion corrections will be explored further in detail in a later section.

For nickel systems, a small number of DFT benchmark studies have been reported in the literature. These included rationalizing the mechanism of Ni-catalyzed processes,[40] analyzing differences in electronic and structural properties of Ni-alkyne complexes for improved catalytic activity and selectivity,[41] and developing a nickel catalyst for CO_2 activation.[42] Studies evaluating the importance of dispersion corrections concluded that these improve results significantly.[43-44]

Functional Taxonomy and Exchange-Correlation Functionals

The tested density functionals may be classified by an order or presentation of exchange-correlation functionals that can be referred to as Perdew's 'Jacob's ladder' of increasing accuracy, represented in Figure 14. Essentially, this is a popular image to illustrate the hierarchy of DFT approximations in that of Jacob's ladder connecting the Earth to Heaven. Each rung represents a different level of approximation that should recover the results of lower rungs in the suitable limits but add more capabilities.[45] Despite its theoretical exactness, in practical calculations, the *N*-body interactions are included in DFT through density functional approximations of the exchange-correlation energy term. Consequently, the accuracy of DFT fully depends on the accuracy of the exchange-correlation energy approximations constructed from the exact quantum mechanical constraints. It is important to know that additional approximations added to the DFT calculations may affect the accuracy of the theoretical predictions and these uncertainties must be considered when interpreting results. A reliable DFT calculation should be characterized by the following relation:

$$Error\ (functional) > Error\ (basis\ set) > Error\ (RI\text{-}J),\ Error\ (grid).$$[37]

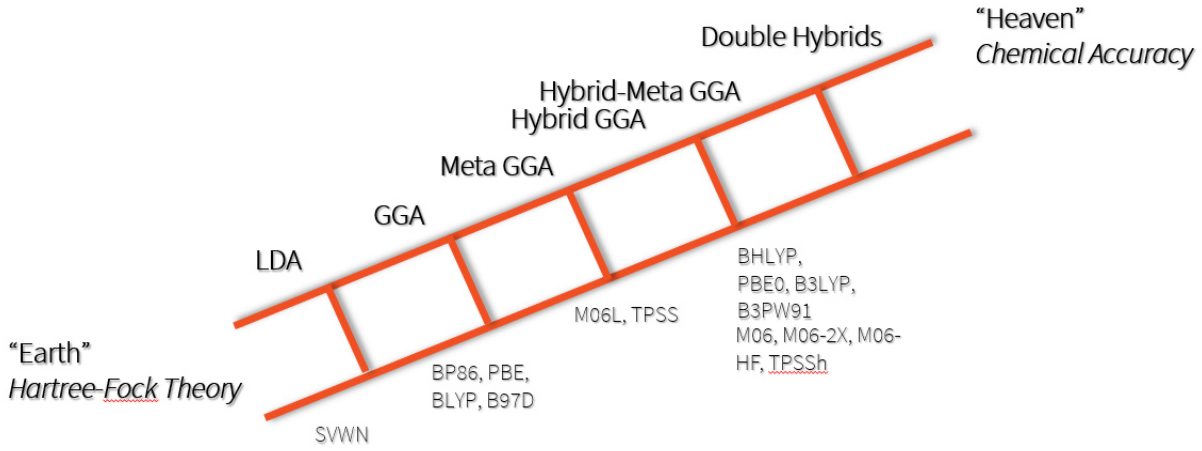

Figure 14. Depiction of Jacob's Ladder with the functionals that was used for the full ligand [Ni(dippe)] DFT calculations

The first and lowermost rung consists of the local spin density approximation (LDSA) in which the density functional depends solely on spin densities. The approximation is represented in eq. (2) where separate local exchange and correlation terms are introduced:

$$E_{\mathrm{xc}}^{\mathrm{LDA}}[n] = E_{\mathrm{x}}^{\mathrm{LDA}}[n] + E_{\mathrm{c}}^{\mathrm{LDA}}[n] \tag{2}$$

The expression for the exchange energy is shown in eq. (3):

$$E_{\mathrm{x}}^{\mathrm{LDA}}[n] = \mathrm{C} \int n^{\frac{4}{3}}(\mathrm{r}) d\mathrm{r} \tag{3}$$

A common functional in this category is called SVWN which requires the Slater exchange functional (S)[46] and the Vosko, Wilk, and Nusair local correlation functional.[47] One may use the SVWN functional as well as other exchange-correlation functionals to complete LSDA calculations for spin-polarized systems. The LSDA functionals are accurate methods and lead to very good predicted molecular geometries; however, bond energies and atomization energies are almost always overestimated compared to experimental data, with quite a large deviation.[48]

The second rung is constituted by the generalized gradient approximation (GGA) where the density functional depends on spin densities and its first derivative in the exchange–correlation potential, the functional reduced gradients. This idea is constructed in the form of eq. (4):

$$E_{\mathrm{xc}}^{\mathrm{GGA}}[n] = \int n(\mathrm{r})\varepsilon_{xc}(n(\mathrm{r}), |\nabla n(r)|)d\mathrm{r} \quad (4)$$

Most functionals including a gradient term are formulated in the form of a correction term which is added to the LSDA functional (eq.5):

$$\varepsilon_{\mathrm{x/c}}^{\mathrm{GGA}}[n] = \varepsilon_{\mathrm{x/c}}^{\mathrm{LDA}}[n] + \Delta\varepsilon_{\mathrm{x/c}}[\frac{|\nabla n(\mathrm{r})|}{n^{\frac{4}{3}}(\mathrm{r})}] \quad (5)$$

In comparison with the LSDA functionals, GGAs mostly improve total energies and atomization energies.[49] One of the most popular exchange-correlation functionals known in this category was proposed in 1988 by Becke (B).[50] As stated in a previous section, DFT functionals contain a self-interaction that is partly corrected by the exchange-correlation term included within the expression. Before, it was rather difficult to formulate exchange functionals to rid this self-interaction, but the Becke functional leads to nearly exact cancellation. Lee, Yang, and Parr also developed a commonly used functional (LYP) that falls within this category and is based on ideas from conventional electronic structure theory relating to electron correlation in terms of the two-electron density matrix. This functional alone predicts a correlation energy of zero for one-electron systems. For example, when calculating the H atom using only the Becke functional and the β-parameter as 0.0042, a Coulomb energy of 0.307 au and an exchange energy of –0.306 au are found, nearly cancelling each other. By combining the Becke and Lee, Yang, and Parr functionals, a quite accurate Coulomb energy for the H atom is obtained of -0.498 au.[51] In this instance, the self-interaction problem of electron-electron interactions that occurs is fixed as it is completely cancelled out.

Besides the functionals mentioned, many other gradient-corrected exchange functionals have been developed from first principles, however some contain different empirical parameters to determine exact data on atoms and small molecules, such as determining the nature of the solutions (e.g. the long-range cancellation of self-interaction).

The functionals corresponding to the third rung include meta-GGA which depend on the second derivative of the total density of the electron (otherwise known as the Laplacian, $\nabla^2 n(\mathrm{r})$) and the spin kinetic energy densities. Common functionals that fall in this category are suggested by Tao, Perdew, Staroverov and Scuseria (TPSS)[52] and the Minnesota functionals, such as M06-L[53] and M11-L.[54] The M06-L functional is intended to work well for calculations involving organometallic molecules. The M11-L functional is an improvement over M06-L as it also is used for organometallic compounds and this functional includes dual-range DFT. Although these functionals are more complex, they do not produce a very large improvement in accuracy over GGA functionals.[55]

The fourth rung is composed of hyper-GGA and hybrid-meta GGA functionals. As discussed previously, the use of local exchange and correlation functionals leads to large overestimations of atomization energies, which is commonly seen when using GGA functionals. On the other hand, the Hartree-Fock method substantially underestimates these same energies. This suggested to researchers that a combination of the two would potentially yield improved results, and this was found to be the case. The general form of these density functionals employ full or partial Hartree-Fock exchange in addition to ingredients from one of the lower rungs, represented in eq. (6):

$$E_{\mathrm{xc}} = (1 - a)E_{\mathrm{xc}}^{\mathrm{DFT}} + aE_{\mathrm{x}}^{\mathrm{HF}} \quad (6)$$

These density functionals have been the most popular choice for chemical applications, and they usually have greater accuracy for chemical problems. One of the most popular examples is the B3LYP 3-parameter functional in which the exchange-correlation energy was expressed as a combination of the local exchange-correlation energy, the HF exchange energy, and the gradient corrections to the exchange and correlation energies[56] as shown in eq. (7):

$$E_{\mathrm{xc}}^{\mathrm{B3LYP}} = (1-a)E_{\mathrm{x}}^{\mathrm{LDA}} + aE_{\mathrm{x}}^{\mathrm{HF}} + b\Delta E_{\mathrm{x}}^{\mathrm{B}} + (1-c)E_{\mathrm{c}}^{\mathrm{LDA}} + cE_{\mathrm{c}}^{\mathrm{LYP}} \quad (7)$$

In comparison to other functionals available at the time of development, this density functional was most impressive. The B3LYP density functional was widely used as it was made swiftly available to the community in numerous popular computational chemistry packages. The original paper by Becke has been cited more than ninety-seven thousand times at the time this thesis was written! This is due to its overall good accuracy for a wide range of applications and was deemed as a 'golden standard' by many experts and experimental scientists. However recently, serious doubts about its usefulness have been raised, especially when considering noncovalent interactions. In 2012, Grimme published an article that discusses the two major shortcomings of B3LYP/6-31G*, namely basis set size and missing dispersion.[73] It has also been found that B3LYP fails to predict the correct mechanism for organic reactions.[74]

There are many other hybrid functionals that have been developed and some have also been widely popularized within the community. These types of functionals are the most popular in comparison to the other categories.

On the fifth and highest rung, we consider double hybrid density functionals (DH) that incorporate correlation energies computed from virtual orbitals. Despite the effort of creating the best hybrid density functional, an important dynamic correlation that is the key of the *ab initio* wavefunction theory (WFT) is absent in density functional correlation energy functionals.

The addition of non-local virtual orbital-dependent terms is shown to overcome many problems of density functional approximations including the top hybrid density functionals.[61] The resulting functionals that were developed by mixing a part of second-order Møller–Plesset (MP2) correlation energy expression are known as the double hybrid density functional approximations, which connect the density functional world with that of the *ab initio* WFT.[62] Originally proposed by Grimme et. al., these functionals are based on mixing of standard GGAs for exchange and correlation with Hartree-Fock exchange and a perturbative second-order correlation part that is obtained from the GGA orbitals and eigenvalues.[57] The general form of this functional is expressed in eq. (8):

$$E^{\mathrm{DFA}} = a_{\mathrm{x}} E_{\mathrm{x}}^{\mathrm{EXX}} + (1 - a_{\mathrm{x}}) E_{\mathrm{x}}^{\mathrm{DFA}} + E_{\mathrm{c}}^{\mathrm{DFA}} \tag{8}$$

Despite the considerable successes behind these functionals, there are limitations that have been further improved by mixing the semilocal correlation functional with the non-local, second order Görling–Levy (GL2) correlation energy expression. The expression for this upgraded functional is shown in eq. (9):

$$E_{\mathrm{xc}}^{\mathrm{DH}} = a_{\mathrm{x}} E_{\mathrm{x}}^{\mathrm{EXX}} + (1 - a_{\mathrm{x}}) E_{\mathrm{x}}^{\mathrm{DFA}} + a_{\mathrm{c}} E_{\mathrm{c}}^{\mathrm{GL2}} + (1 - a_{\mathrm{c}}) E_{\mathrm{c}}^{\mathrm{DFA}} \tag{9}$$

With these additional corrections, the improvement of *N*-electron self-interaction problems and non-covalent interactions are visible. Unfortunately, these methods have a substantial computational cost, which prevents researchers from constructing usable functionals with higher perturbation terms such as triple and quadruple hybrids. Also, researchers typically avoid adding these higher terms to the energy since there is no guarantee that a perturbation expansion will show nice convergence behavior for a given problem, and one may have large terms that partially cancel out to yield large errors. However, MP2 does not generally have these issues.

We were unable to incorporate these functionals in the benchmarking of both [Ni(dmpe)] and [Ni(dippe)] systems due to the large costs. The error message we kept receiving was labeled as a memory error.

Dispersion Interactions in DFT

Dispersion interactions occur from the attractive part of a van der Waals-type interaction potential between atoms that are not directly bonded to each other.[56] In other words, London dispersion interactions result from relatively long-ranged electron correlation effects in any many-electron system. In the case of organometallic complexes, dispersion forces are certainly present between different parts of the molecule. Most common density functionals do not account for these interactions that may occur within the given systems. This could result in altered geometries at the active site and the calculated energetics for both dissociation of a bulky ligand and other reactions may be incorrect. Researchers found evidence that such effects are important and the absence of dispersion in DFT computations accounts for a large change in bond energy predictions.[34]

For dispersion-corrected density functionals, a molecular mechanics term is added to the energy to improve the treatment of dispersion interactions and their medium-range continuations. A different approach to including empirical dispersion corrections in DFT are the Minnesota functionals, which include many additional parameters into the exchange-correlation functional to reproduce dispersion effects.

To summarize, current DFT functionals provide unexpected accuracy for a low computational cost, however they do still lead to significant errors.

Which functional should you choose?

After completing an extensive background search on which functionals would be the best for the significant chemical system being studied, the question constantly asked was, "Which functional should I choose?"

It has been examined that in theory, the DFT approach is exact and produces the exact ground-state energy and density. However, in practice one must use approximations on the exchange-correlation energy. The quality of the results obtained highly depend on the quality of the approximations used. Much of current DFT research is dedicated to developing such approximations. Unfortunately, there is currently no systematic approach in place, and so hundreds of different functionals have been proposed. This has left the bemused user to ask the question.

In any practical instance, the choice of functional strongly depends on the chemical system being observed. Due to the diversity of bonding situations in inorganic chemistry, ranging from covalently bonded isolated molecules to ionic crystals and metal clusters, a uniformly and usefully accurate approximate DFT description for all these systems is not yet available.[37] This idea is what led to the benchmarking study for the [Ni(dippe)] system being investigated.

Computational Details

DFT calculations were performed on Lonestar5 and Stampede2 supercomputers located at the University of Texas at Austin, Texas Advanced Computing Center. As a starting point, we used the previously published structures located in the computational modelling of the C—CN bond activation of the benzonitrile, using [Ni(dmpe)] fragment, as a model for [Ni(dippe)]. For

this study, we modified these structures by adding the fluoro substituents. The gas phase structures were fully optimized in redundant internal coordinates,[64] with density functional theory (DFT) and a wave function incorporating Becke's three-parameter hybrid functional (B3),[56] along with the Lee-Yang-Parr correlation functional (LYP).[51] All calculations were performed using the Gaussian16 package.[65] The Ni and P atoms were represented with the effective core pseudopotentials of the Stuttgart group and the associated basis sets improved with a set of *f*-polarization functions for Ni ($\alpha = 3.130$)[66] and a set of *d*-polarization functions for P ($\alpha = 0.387$).[67] The remaining atoms (C, H, and N) were represented with 6-31G(d,p)[68] basis sets. The geometry optimizations were performed without any symmetry constraints, and the local minima and the transition states were checked by frequency calculations. Zero-point energies, thermal corrections, entropic corrections were all considered and calculated from the frequency calculations. The solvent effects on the relative stability of the structures were evaluated by calculating the free energies of solvation using solvent model density (SMD)[69] for the gas-phase-optimized structures with 6-311++G(d,p) basis sets[70] for C, H and N. The energies mentioned throughout this thesis are the solvation corrected Gibbs free energies calculated at 298.15K and 1 atm, which are calculated by the following equation:

$$G\left(\frac{kcal}{mol}\right) = (qhG(T) - E + SPE)\ x\ 627.5 \qquad (10)$$

The value (*qhG(T)-E)* is obtained using Truhlar's quasi-harmonic approximation.[71] The value *E* is the electronic energy and *SPE* is solvent corrected electronic energy.

The Chimera package was used to display the molecular structures.[72]

CHAPTER IV

RESULTS AND DISCUSSION

Interatomic Distances and Bond Angle Analysis

The DFT calculations show in Figure 15 that the C—N and phenyl group are located in the same plane for the η^2 complex. Table 1 shows that all the Ni—CN bond distances observed are longer than the C, N triple bond. It is important to establish that for the η2 complexes, the CN bond lies in the same plane as the phenyl ring. There are no notable deviations among the bond lengths and bond angles in this case, which show that the independent variable will be the fluoro substituent. The C—CN bond lengths showed an average bond distance of 1.465 Å with a deviation of ± 0.005 Å. The Ni—CN bond lengths had an average value of ~1.87 Å with the 2-fluoro and 2,6-difluoro molecules containing a 1.86 Å bond length. Ni—$C\alpha_{aryl}$ bond angles measured 3.23 Å for all except the 2,6-difluoro complex, which measured 3.21 Å. The Ni—Cαaryl bond distances had the largest range spanning from 3.81-3.89 Å. All bond angles between the Ni—CN—C_{aryl} complexes were ~150° with the 2-fluoro molecule observing a deviation at 152.05°. All bond lengths for each of the important bonds followed the trend: Ni—$C\alpha_{aryl}$ > Ni—C_{aryl} > Ni—CN> C—CN for all fluorinated η^2-benzonitrile [Ni(dmpe)] complexes. Since are no notable differences between bond lengths or angles, this allowed for the comparison of the η^2 complexes.

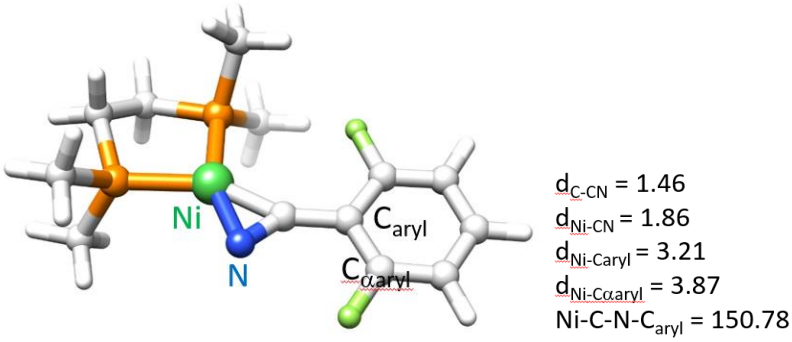

Figure 15: η^2-nitrile complex of [Ni(dmpe)] with 2,6-difluorobenzonitrile.

Table 1: Selected Interatomic Distances (in Å) for η^2-CNs Involved in C—C Bond Activation calculated by using Gaussian16, B3LYP/C, H, N, F (6-31G**), Ni, P (SDDALL) α_{Ni} = 3.130, α_P = 0.387/SMD (toluene/THF).

	$d_{C\text{-}CN}$	$d_{Ni\text{-}CN}$	$d_{Ni\text{-}Caryl}$	$d_{Ni\text{-}C\alpha aryl}$	Bond Angle (Ni-C-N-C_{aryl})
H	1.47	1.87	3.23	3.82	150.14
2F	1.46	1.86	3.23	3.89	152.05
3F	1.47	1.87	3.23	3.81	150.34
4F	1.46	1.87	3.23	3.83	150.43
26F2	1.46	1.86	3.21	3.87	150.78
35F2	1.47	1.87	3.23	3.81	150.79

In the case of the oxidative addition product, Figure 16 shows that the aryl plane is perpendicular to the P-Ni-P and Ni—C_{aryl} planes, which is consistent with the 2,6-difluorosubstrate. Again, the bond lengths did not show significant differences between one another as seen in Table 2. The C—CN bond lengths were all 2.73 Å with the 2,6-diflouro complex having a 2.75 Å bond length. The Ni—CN bond lengths were all measured at 1.87 Å. The Ni—C_{aryl} bonds measured at ~2.90 Å with the 2-fluoro complex having a slightly shorter bond length of 2.87 Å. The C—CN interatomic distance increased due to the nature of the

oxidative addition reaction. The increased oxidation number of the nickel caused the two atoms to distance themselves, thus creating the most stable structure. All bond lengths followed the trend: Ni—Cα_{aryl} > C—CN >Ni—C$_{aryl}$ > Ni—CN. There were no notable differences when comparing the bond distances, therefore the energies of the oxidative addition fluorobenzonitrile [Ni(dmpe)] complexes can be compared.

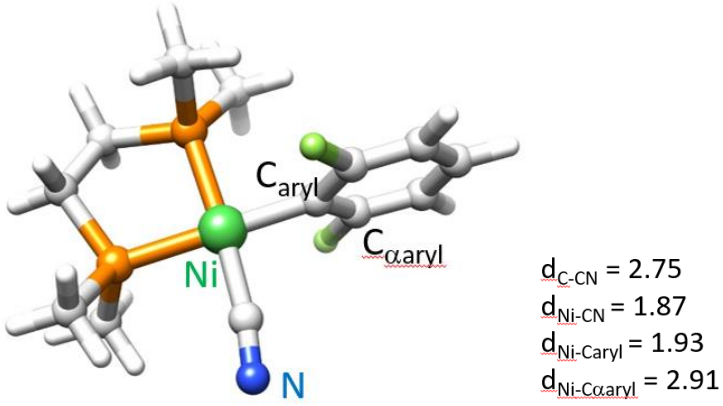

Figure 16: C—C bond activation product of the reaction of [Ni(dmpe)] with 2,6-difluorobenzonitrile.

Table 2: Selected Interatomic Distances (in Å) for OA products calculated by Gaussian16, B3LYP/C, H, N, F (6-31G**), Ni, P (SDDALL) α_{Ni} = 3.130, α_P = 0.387/SMD (toluene/THF).

	$d_{C\text{-}CN}$	$d_{Ni\text{-}CN}$	$d_{Ni\text{-}Caryl}$	$d_{Ni\text{-}C\alpha aryl}$	ΔG (kcal/mol)
H	2.73	1.87	1.92	2.91	5.41
2F	2.73	1.87	1.92	2.87	0.59
3F	2.73	1.87	1.92	2.90	4.36
4F	2.73	1.87	1.93	2.91	5.28
26F2	2.75	1.87	1.93	2.91	-6.15
35F2	2.73	1.87	1.92	2.90	3.13

The transition state (TS) complex, (along with labeled atoms involved in the C—C bond formation) can be seen with the 2,6-difluorobenzonitrile Ni(dmpe) complex in Figure 17. The single point energy calculations in Table 3 show the bond lengths involved in C—C bond formation of the TS complexes. Much of the C—CN bond lengths are within the range of 1.56-1.59 Å apart from the 2,6-fluoro benzonitrile complex. The Ni—CN bonds of the TS were measured in the range of 1.87-1.88 Å, again with an exception of the 2,6-fluoro substrate. The Ni—C_{aryl} bond distances were measured in a range of 2.01-2.04 Å with the 2,6-fluoro TS structure observing a minor difference of 2.07 Å. The Ni—$C_{\alpha aryl}$ bond lengths were measured in a wider range of 2.70-2.75 Å, with outliers occurring with both 2,6- and 3,5-difluoro complexes. As seen from the results, the 2,6-difluoro bond lengths are constantly outliers compared to the other fluorinated benzonitrile bond lengths. The differences in these bond lengths can be described by the steric interactions caused by the two *o*-fluoro groups positioned near the Ni metal center in the [(Ni(dmpe)] complex. Even with this difference, the bond lengths of the TS structures show a clear trend: Ni—$C\alpha_{aryl}$ > Ni—C_{aryl} >Ni—CN> C—CN. For all bond length analysis, no major outliers were observed. According to Hammond's postulate, the more stable product should have a more stable transition state. This suggests that the activation energy of a step will be inversely proportional to the stability of the product.[75] Unexpectedly though, that isn't the case here.

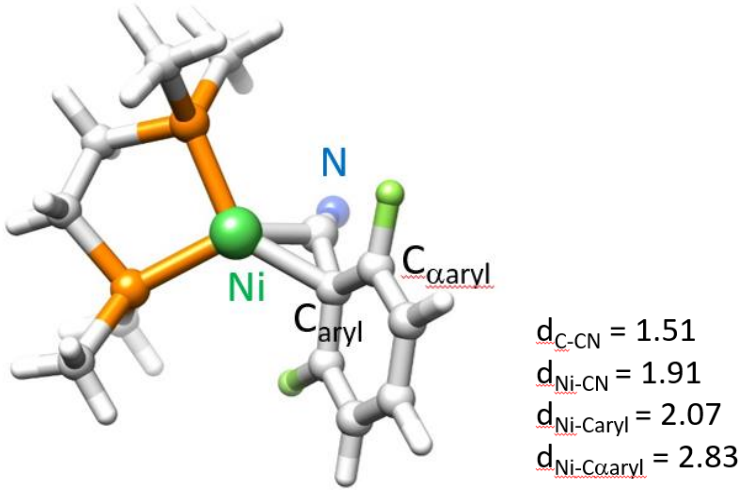

Figure 17: Transition state structure for the C—C bond activation of 2,6-difluorobenzonitrile with [Ni(dmpe)].

Table 3: Selected Interatomic Distances (in Å) for TSs Involving in C—C Bond Activation calculated by Gaussian16, B3LYP/C, H, N, F (6-31G**), Ni, P (SDDALL) α_{Ni} = 3.130, α_P = 0.387/SMD (toluene/THF).

	$d_{C\text{-}CN}$	$d_{Ni\text{-}CN}$	$d_{Ni\text{-}Caryl}$	$d_{Ni\text{-}C\alpha aryl}$	$\Delta G^{\ddagger}$ (kcal/mol)
H	1.59	1.88	2.04	2.75	28.07
2F	1.57	1.88	2.01	2.75	27.51
3F	1.58	1.88	2.03	2.70	28.25
4F	1.59	1.87	2.04	2.76	28.39
26F2	1.51	1.91	2.07	2.83	27.59
35F2	1.57	1.88	2.03	2.66	28.11

Predicted *o*-Fluorine Effect

There is a very good correlation between the Gibbs free energies (ΔG) and the number of *o*-fluoro substituents both in toluene and THF (Figure 18). The stabilization of the oxidative addition product is 6.6 kcal/mol for each *o*-fluoro substituent.

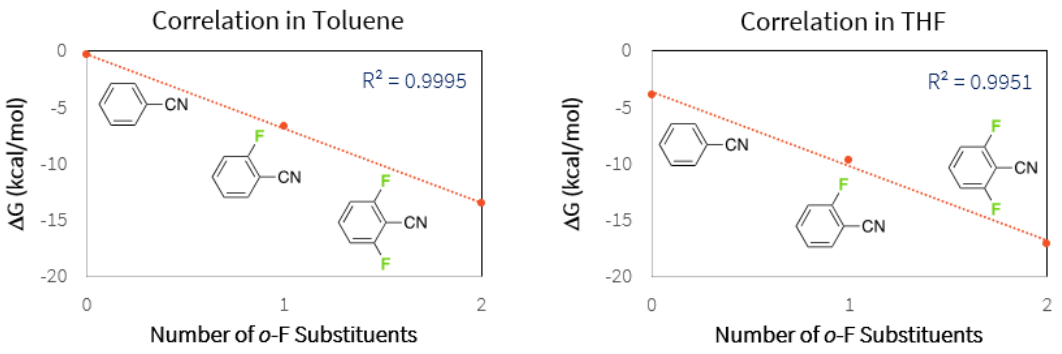

Figure 18: Predicted *o*-Fluorine Effect on Calculated ΔG Values by using Gaussian16, B3LYP/C, H, N, F (6-31G**), Ni, P (SDDALL) α_{Ni} = 3.130, α_P = 0.387/SMD (toluene/THF).

The correlation of reductive elimination activation barriers with respect to the number of o-F substituents show a good correlation with R^2 values of 0.985 and 0.9773 in toluene and THF, respectively (Figure 19). There is a 7.3 and 7.7 kcal/mol increase in the reductive elimination activation barriers per *o*-fluoro substituent.

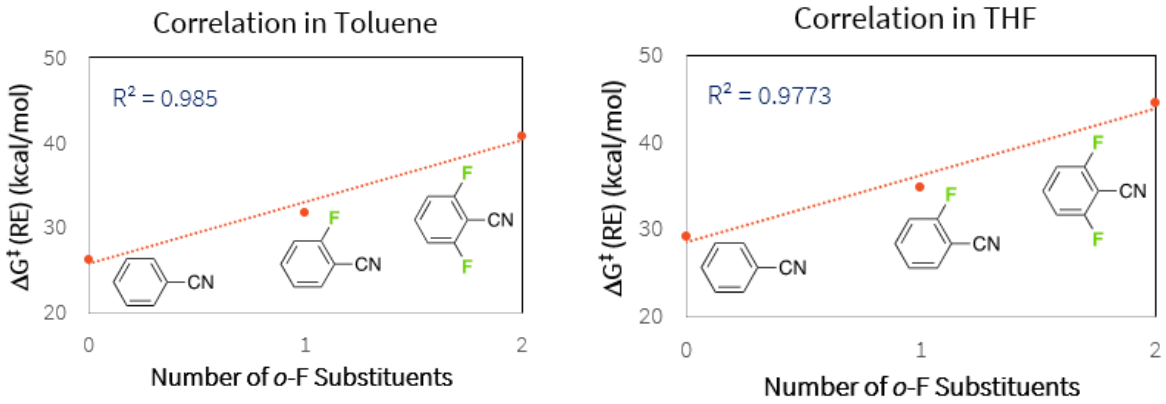

Figure 19: Predicted *o*-Fluorine Effect on Calculated $\Delta G^{\ddagger}$ (RE) Values by using Gaussian16, B3LYP/C, H, N, F (6-31G**), Ni, P (SDDALL) α_{Ni} = 3.130, α_P = 0.387/SMD (toluene/THF).

There was only reliable equilibrium constant experimental data obtained for the 3F, 4F and benzonitrile substrates. For the others, there was not enough η^2-nitrile in solution to measure

a reliable equilibrium constant. When we compared the energies obtained from the Van't Hoff plots with those calculated with [Ni(dmpe)] (Table 4), there is a very good correlation between the calculated values and the experimental values.

Table 4: A comparison of the experimental ΔG values obtained from the Van't Hoff plots and the calculated ΔG values with [Ni(dmpe)] by using Gaussian16/ B3LYP/C, H (6-31G**); Ni, P (SDDALL) α_{Ni} = 3.130, α_P = 0.387/SMD (toluene/THF).

	ΔG	ΔG*
3-FC_6H_4CN (THF)	-2.38	-5.6
3-FC_6H_4CN (Tol)	-1.23	-1.9
4-FC_6H_4CN (THF)	-1.16	-4.5
4-FC_6H_4CN (Tol)	-0.51	-0.9
C_6H_5CN (THF)	-0.76	-3.9
C_6H_5CN (Tol)	-0.11	-0.4

Energies in kcal/mol

Energy analysis

The results from DFT calculations in Table 5 show that the energy difference between the oxidative addition products and η^2 nitrile complexes showed dependence on the number of *o*-fluoro substituents. However, the 3F, 4F and 3,5-difluoro substituents did not affect the energy values as much as the *o*-F substituents.

Table 5: DFT Calculations with [Ni(dmpe)] Complexes. Energies are in kcal/mol and calculated by using Gaussian16, B3LYP/C, H, N, F (6-31G**), Ni, P (SDDALL) $\alpha_{Ni} = 3.130$, $\alpha_P = 0.387$/SMD (toluene/THF).

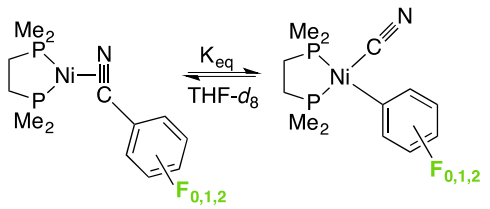

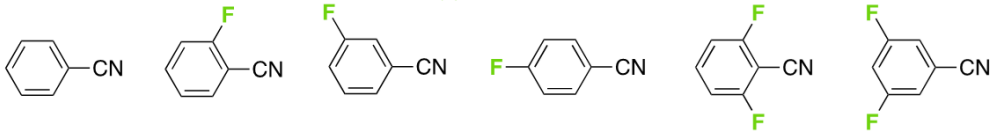

ΔG (Tol)	-0.4	-6.7	-1.9	-0.9	-13.5	-3.6
ΔG (THF)	-3.9	-9.7	-5.6	-4.5	-17.1	-7.4
$\Delta G^{\ddagger}$ OA (Tol)	26.0	25.3	26.1	26.3	27.3	26.1
$\Delta G^{\ddagger}$ OA (THF)	25.2	25.2	25.4	25.5	27.5	25.5
$\Delta G^{\ddagger}$ RE (Tol)	26.3	32.0	28.0	27.2	40.8	29.7
$\Delta G^{\ddagger}$ RE (THF)	29.1	34.8	31.0	30.0	44.6	33.0

The non-fluorinated complex showed an energy value of 0.4 kcal/mol in THF and 3.9 kcal/mol in toluene. The 4-fluoro complex had a slightly more stable energy value of 0.9 and 4.5 kcal/mol in THF and toluene. The 3-fluoro complex was more stable, giving a 1.9 and 5.6 kcal/mol energy value in THF and toluene, respectively. The 2-fluoro complex gave a 6.7 kcal/mol energy value in THF and a 9.7 kcal/mol value in toluene. The 3,5-diflourinated complex was less stable than the single ortho-fluoro complex with values of 3.6 and 7.4 kcal/mol in THF and toluene, respectively. Finally, the 2,6-difluoro complex was the most stable with energy values of 13.5 and 17.1 kcal/mol in THF and toluene, respectively. In Figure 20, we see that the number of *o*-fluoro groups do affect the stability of the oxidative addition products. The results show a strong trend, aligning with the ortho-fluoro effect. The two most stable complexes are the ortho-fluorinated benzonitrile complexes. It is interesting to note that the 3,5-difluoro

complex was more stable than other non-ortho fluoro complexes. These results indicate that the number of fluorine may influence the stability of the complex, but this is overshadowed by the ortho-fluoro effect.

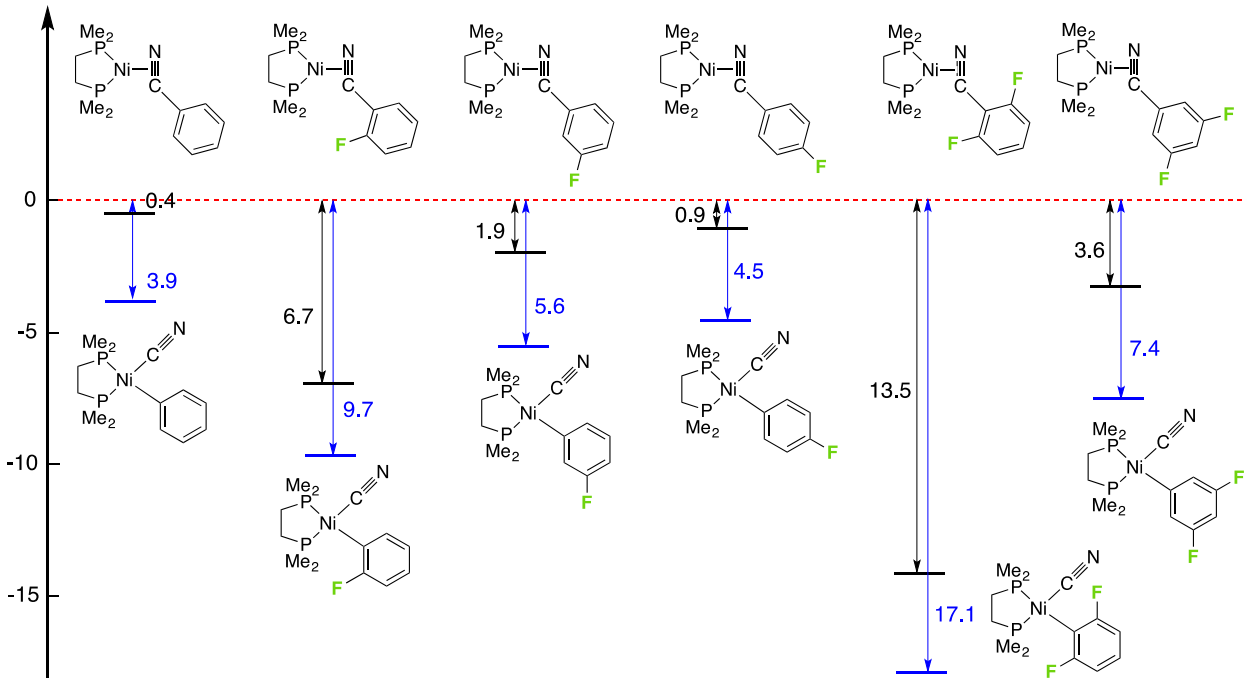

Figure 20: ΔG (kcal/mol) calculated for the C—CN bond activation reaction by using Gaussian16, B3LYP/C, H, N, F (6-31G**), Ni, P (SDDALL) α_{Ni} = 3.130, α_P = 0.387/SMD (toluene/THF).

The TS energy values calculated for the C—CN bond activation reaction are shown in Figure 21. The activation barriers for the C—C bond activation are nearly identical and the energies for the oxidative addition transition states do not show much variation between complexes. The energies of the C—CN bond activation transition states are constant, ranging from 25.2-25.5 kcal/mol for energies in the THF solution. The 2,6-difluoro complex was the only complex outside of this range with a value of 27.3 kcal/mol. The complexes in toluene solution showed a slightly larger range of 25.3-27.3 kcal/mol. The 2,6-difluoro complex had the highest

value in the range while the 2-fluoro complex was the lowest value in the range. The slightly higher transition state energy for 2,6-difluoro could be the result of the significant steric effects of the fluoro groups on the 2,6-difluorobenzonitrile. All the transition states contain similar energy values, although the *o*-fluoro substrates observed more stable oxidative addition end products

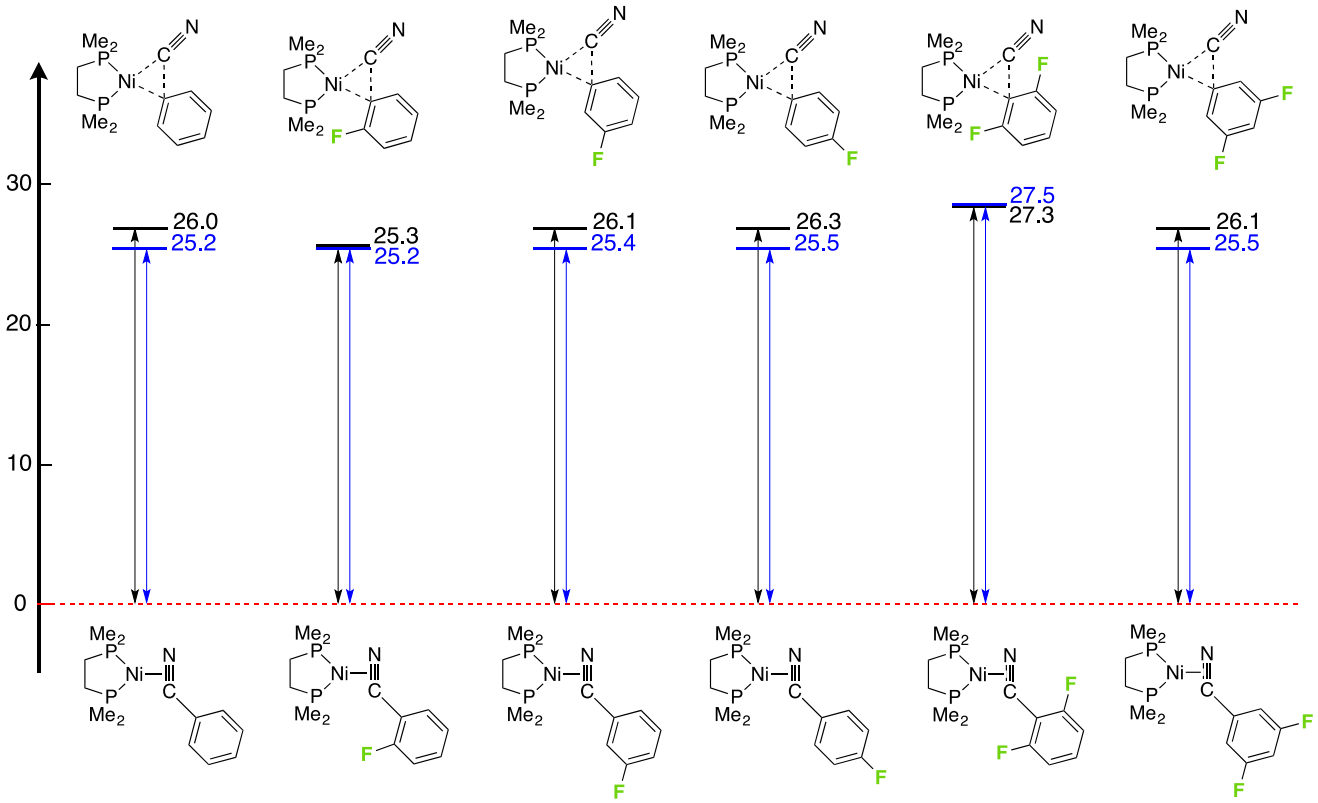

Figure 21: $\Delta G^{\ddagger}$ (kcal/mol) calculated for the C—CN bond activation reaction by using Gaussian16, B3LYP/C, H, N, F (6-31G**), Ni, P (SDDALL) $\alpha_{Ni} = 3.130$, $\alpha_{P} = 0.387$/SMD (toluene/THF).

The energy values calculated for the C—CN reductive elimination are shown in Figure 22. These results show a very strong correlation with the number of *o*-fluoro substituents. All energy values are larger when compared to the forward reactions, indicating a much slower

reverse reaction rate. The 2,6-difluoro complex show energy values of 40.8 kcal/mol in THF and 44.6 kcal/mol in toluene. The 2-fluoro complex give values of 32.0 kcal/mol in THF and 34.8 kcal/mol in toluene. Both *o*-fluoro complexes have larger energy values compared to the 26.3-29.7 and 29.1-33.0 kcal/mol range of the non-ortho fluorinated complexes in THF and toluene. With these calculations, there is only a significant change with the 2-F and 2,6-difluoro substrates. Therefore, further analysis was completed with the benzonitrile, 2-F and 2,6-difluoro benzonitriles. Looking at the reverse reaction, the reductive elimination of the C—CN bond, the energies for C—C reductive elimination show a very good correlation with the number of *o*-F substituents. As discussed previously, these energies are affected mostly by the relative stability of the oxidative addition products, and that is observed once more with the 2-F and 2,6-difluoro benzonitriles.

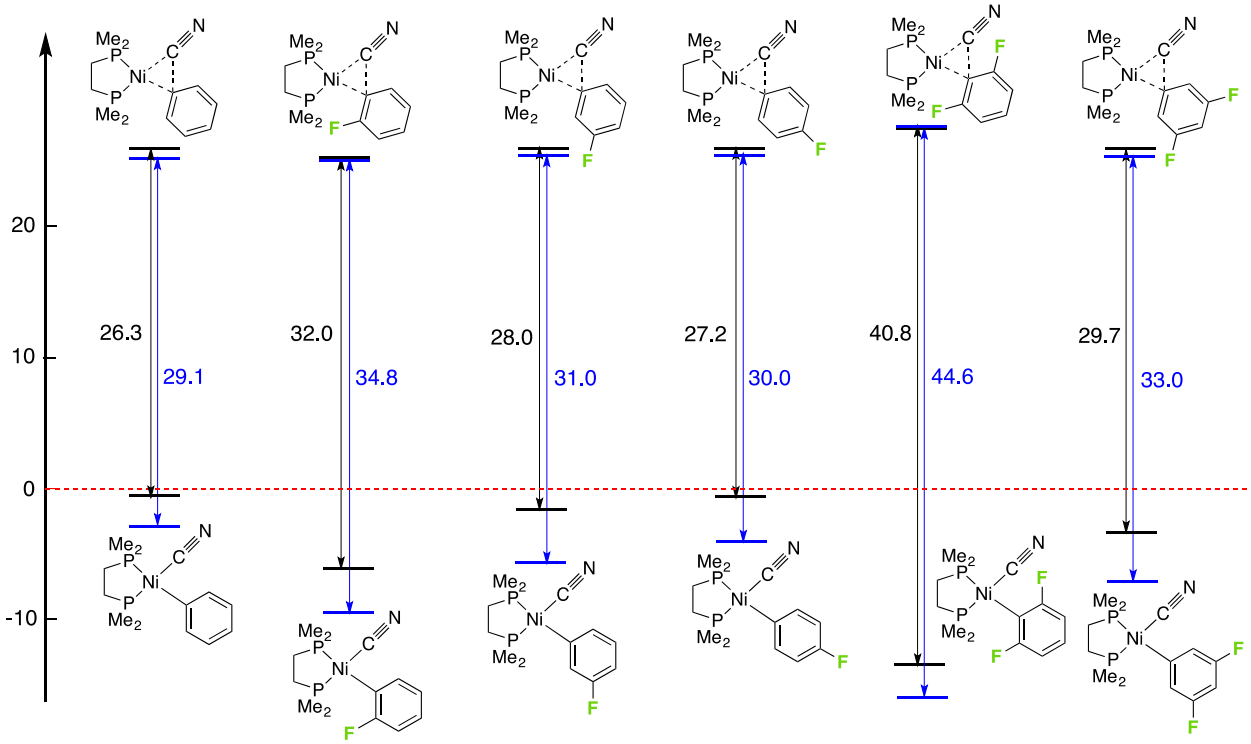

Figure 22: $\Delta G^{\ddagger}$ (kcal/mol) calculated for the C—CN reductive elimination by using Gaussian16, B3LYP/C, H, N, F (6-31G**), Ni, P (SDDALL) α_{Ni} = 3.130, α_{P} = 0.387/SMD (toluene/THF).

DFT benchmark analysis

As the next step, we started the DFT analysis with the full ligand using [Ni(dippe)]. The most optimal functionals for our DFT calculations with the [Ni(dippe)] fragment were determined by a thorough benchmarking study. After extensive background research, it was initially believed that current functionals (such as M06) would prove to perform better in comparison to older methods such as B3LYP. In our case with [Ni(dippe)] however, this was not the case. By performing the benchmark study on our most stable conformations, 36 density functionals were considered as shown in Table 6.

Table 6: Functionals that were used for full ligand DFT calculations and their reported energies. ΔG is reported in kcal/mol calculated by using Gaussian16/C, H (6-31G**); Ni, P (SDDALL), α_{Ni} = 3.130, α_P = 0.387/SMD (toluene/THF).

	ΔG (thf)	ΔG (tol)	ΔG(thf)/ΔG(tol)
Expt	-1.16	-0.51	2.3
B3LYP-GDBJ3	-8.26	-3.61	2.3
B3LYP-GD3 (qh)	-7.72	-3.20	2.4
CAM-B3LYP GD3 (qh)	-7.89	-3.20	2.5
B3LYP	-1.00	2.90	-0.3
M06	-2.22	1.63	-1.4
M06-GD3 (qh)	-4.32	-0.11	37.8
SVWN (qh)	4.65	8.07	0.9
M06L	-0.56	3.81	-0.2
M06L GD3	-0.22	4.07	-0.1
M11L (qh)	-1.02	2.71	-0.4
TPSSTPSS (qh)	2.20	6.15	0.4
TPSSTPSS GD3BJ	-1.8	2.19	-0.8
B3PW91	1.64	5.61	0.3
B3PW91 GD3BJ (qh)	-6.33	-1.51	4.2
B97D	-2.42	1.76	-1.4
B97D3	-1.60	1.98	-0.8
BLYP	1.88	6.23	0.3
BLYP GD3BJ (qh)	-6.59	-2.04	3.2
BP86	4.10	8.43	0.5
BP86 GD3BJ	-2.62	0.61	-4.3
PBEPBE	4.33	8.59	0.5
PBEPBE GD3BJ	-25.2	4.27	-5.9
B3P86	1.67	3.09	0.5
M06-HF (qh)	-31.7	-30.2	1.1
M06-HF GD3	-31.9	-29.8	1.1
TPSSH	1.75	5.52	0.3
M11	-11.1	-6.59	1.7
CAM-B3LYP	-2.75	1.60	-1.7
CAM-B3LYP GD3BJ	-7.10	-3.63	2.0
HF	-35.8	-34.0	1.1
MPW1PW91	0.62	4.13	0.2
PBE1PBE	1.00	2.14	0.5
PBE1PBE GD3BJ	-3.06	0.33	-9.2
BHandHLYP	-9.94	-4.48	2.2
M06-2X	-12.0	-7.00	1.7
M06-2X GD3	-11.3	-7.40	1.5

The importance of dispersion effects is evident when we inspect the two most stable conformers that are also observed in the X-ray crystal structures. On one side of the [Ni(dippe)] ligand, there is a C—H aryl interaction (Figure 23), whereas the other side of the [Ni(dippe)] ligands show variation of the isopropyl group orientations (Figure 24). The ΔG values calculated for the [Ni(dmpe)] complexes using the most popular B3LYP functional are very close to the experimentally measured values for each of the fluorinated substituents. Interestingly, it did not perform as well as for the [Ni(dippe)] complexes presumably due to the dispersion effects.

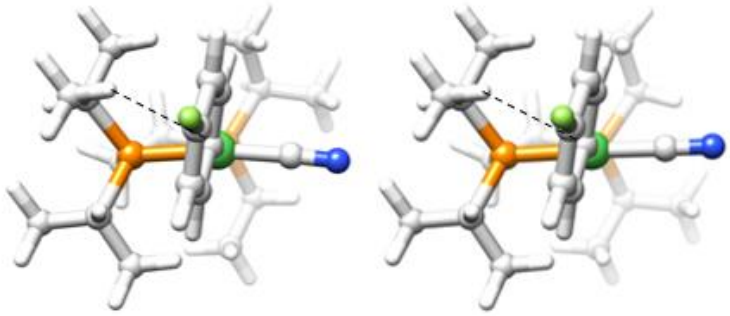

Figure 23: C—H aryl interactions observed in the [Ni(dippe)] ligand.

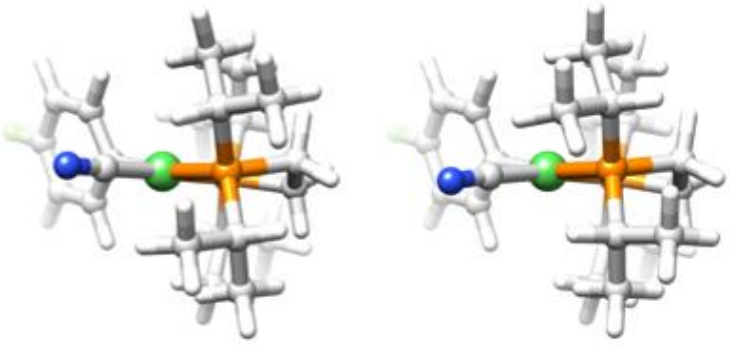

Figure 24: Variation of the isopropyl group orientations observed in the [Ni(dippe)] ligand. These are also the two most stable [Ni(dippe)] conformers.

For each of the functionals employed, the energetics, zero-point energy calculations, enthalpy, entropy, and thermal corrections were calculated for the η^2 complexes and oxidative addition products which are seen in Tables 7-10. To determine the best performing functionals for our study, the energies and their ratios were compared for each functional with the experimental values of 4-fluorobenzonitrile. The energy values for the reaction were calculated in THF and toluene using SMD. The products in THF should theoretically be more stable than those in toluene. A requirement for a "best performing functional" was to ensure the THF energy value was more negative than the same calculation in toluene. Another requirement was to have a similar ΔG ratio when compared to the experimentally measured value of 2.1. The methods which contained a ratio (ΔG(THF): ΔG(toluene)) between 2.1 and 2.5 were valid. The results from DFT calculations show that B3LYP with added dispersion corrections was the closest to the experimental data. M06 for instance, already has dispersion in it, and yet this functional gave opposite selectivity for the η^2 nitrile complex. When adding the empirical dispersion and quasi-harmonic corrections to this functional, it still did not perform as well, i.e. it overestimated the solvation effects. The best performing functionals for the C—CN bond activation reactions with the [Ni(dippe)] fragment was determined to be B3LYP-GDBJ3, B3LYP-GD3 and CAM-B3LYP GD3. These functionals are a form of the most popular B3LYP function with added empirical dispersion corrections. Remarkably, the B3LYP functional did not perform as well without corrections applied. Although, B3LYP is a popular functional with reasonable accuracy, it does not work well without the dispersion corrections.

Table 7: Table energetics, zero-point energy calculations, enthalpy, entropy, and thermal corrections for each DFT method.

*Best performing methods are **bolded** (B3LYP GD3BJ, B3LYP GD3, CAM-B3LYP GD3). All ΔG units measured in (kcal/mol)

Method	**E/au**	**ZPE/au**	**H/au**	**T.S/au**	**T.qh-S/au**	**G(T)/au**	**qh-G(T)/au**
SVWN	-1155.557176	0.515643	-1155.007305	0.09862	0.092361	-1155.105924	-1155.099666
	-1155.553415	0.516382	-1155.002795	0.098967	0.092461	-1155.101762	-1155.095256
	-1155.544566	0.515034	-1154.995169	0.096434	0.091946	-1155.091603	-1155.087115
	-1155.535853	0.515543	-1154.985889	0.096679	0.092094	-1155.082569	-1155.077983
M06L	-1160.583069	0.529667	-1160.019437	0.098517	0.092056	-1160.117954	-1160.111493
	-1160.580088	0.530331	-1160.015856	0.098197	0.091942	-1160.114053	-1160.107798
	-1160.580063	0.528322	-1160.017199	0.098219	0.092791	-1160.115419	-1160.10999
	-1160.571422	0.529404	-1160.007717	0.097268	0.092287	-1160.104985	-1160.100004
M06L GD3	-1160.590189	0.529565	-1160.026583	0.099257	0.092378	-1160.125841	-1160.118962
	-1160.587201	0.530192	-1160.023002	0.099055	0.092325	-1160.122058	-1160.115327
	-1160.587772	0.528403	-1160.024879	0.09789	0.092628	-1160.122769	-1160.117507
	-1160.579121	0.529443	-1160.01539	0.097199	0.092248	-1160.112589	-1160.107637
M11L	-1160.67081	0.5218	-1160.115415	0.096805	0.091012	-1160.212221	-1160.206427
	-1160.667284	0.522375	-1160.111276	0.097336	0.091258	-1160.208613	-1160.202535
	-1160.669942	0.521131	-1160.114929	0.095199	0.090967	-1160.210128	-1160.205896
	-1160.660687	0.521626	-1160.105116	0.095606	0.09117	-1160.200721	-1160.196285
TPSSTPSS	-1160.788808	0.523134	-1160.230929	0.100642	0.093741	-1160.331571	-1160.32467
	-1160.785913	0.52369	-1160.227482	0.100776	0.093783	-1160.328258	-1160.321266
	-1160.779696	0.522142	-1160.222305	0.099871	0.094204	-1160.322177	-1160.31651
	-1160.771282	0.522718	-1160.21334	0.100108	0.094213	-1160.313448	-1160.307553
TPSSTPSS GD3BJ	-1160.909694	0.524019	-1160.351145	0.099754	0.093174	-1160.450899	-1160.444319
	-1160.906672	0.524496	-1160.347627	0.099924	0.093271	-1160.447552	-1160.440898
	-1160.908865	0.523041	-1160.350868	0.098476	0.093426	-1160.449344	-1160.444294

	-1160.900351	0.523805	-1160.341675	0.098642	0.093414	-1160.440317	-1160.43509
B3LYP	-1160.664997	0.530495	-1160.100496	0.099233	0.092377	-1160.199729	-1160.192874
	-1160.661409	0.531093	-1160.096342	0.099165	0.092325	-1160.195507	-1160.188668
	-1160.662367	0.529628	-1160.098293	0.0979	0.092581	-1160.196193	-1160.190874
	-1160.653357	0.530227	-1160.088725	0.097845	0.09247	-1160.18657	-1160.181195
B3LYP GD3BJ	**-1160.824169**	**0.531921**	**-1160.258574**	**0.097504**	**0.091369**	**-1160.356078**	**-1160.349943**
	-1160.820406	**0.53238**	**-1160.254316**	**0.097764**	**0.091526**	**-1160.35208**	**-1160.345842**
	-1160.831456	**0.530564**	**-1160.266575**	**0.097796**	**0.092378**	**-1160.364371**	**-1160.358954**
	-1160.822301	0.531579	-1160.256601	0.097095	0.091942	-1160.353697	-1160.348544
B3PW91	-1160.389759	0.531166	-1159.824615	0.098993	0.092289	-1159.923608	-1159.916904
	-1160.385829	0.53172	-1159.820101	0.09925	0.092382	-1159.919352	-1159.912484
	-1160.38278	0.530074	-1159.818221	0.09809	0.092716	-1159.916311	-1159.910937
	-1160.373478	0.530705	-1159.808306	0.09805	0.092639	-1159.906357	-1159.900945
B3PW91 GD3BJ	-1160.556258	0.532486	-1159.990144	0.097289	0.091273	-1160.087434	-1160.081418
	-1160.552201	0.533087	-1159.985476	0.097575	0.091372	-1160.083051	-1160.076848
	-1160.559964	0.530886	-1159.994741	0.097316	0.092321	-1160.092057	-1160.087062
	-1160.550581	0.531989	-1159.98538	0.094039	0.089983	-1160.079419	-1160.075362
B3LYP GD3	**-1160.751758**	**0.531914**	**-1160.186359**	**0.096873**	**0.090918**	**-1160.283232**	**-1160.277277**
	-1160.748033	**0.532251**	**-1160.182227**	**0.097473**	**0.091236**	**-1160.279701**	**-1160.273463**
	-1160.758489	**0.531125**	**-1160.193497**	**0.096071**	**0.091246**	**-1160.289567**	**-1160.284742**
	-1160.749335	0.532117	-1160.183535	0.095536	0.090895	-1160.27907	-1160.274429
B97D	-1160.482082	0.516714	-1159.930856	0.099143	0.092801	-1160.029999	-1160.023657
	-1160.478942	0.518406	-1159.926256	0.098367	0.092323	-1160.024623	-1160.018579
	-1160.48261	0.516063	-1159.931712	0.098163	0.093043	-1160.029875	-1160.024755
	-1160.47379	0.517394	-1159.921928	0.096661	0.092143	-1160.018588	-1160.014071
B97D3	-1160.577127	0.521301	-1160.021529	0.098782	0.092489	-1160.12031	-1160.114017
	-1160.574137	0.521789	-1160.018024	0.099064	0.092633	-1160.117088	-1160.110657

	-1160.576118	0.520664	-1160.020744	0.097954	0.092889	-1160.118698	-1160.113633
	-1160.567362	0.520997	-1160.011542	0.098962	0.093313	-1160.110504	-1160.104855
	-1160.044444	0.515209	-1159.494361	0.100655	0.093844	-1159.595016	-1159.588205
BLYP	-1160.041852	0.515767	-1159.491222	0.101058	0.09401	-1159.59228	-1159.585231
	-1160.036761	0.514549	-1159.486889	0.099958	0.094276	-1159.586847	-1159.581164
	-1160.028652	0.514991	-1159.478336	0.099838	0.094216	-1159.578174	-1159.572552
BLYP GD3BJ	-1160.234818	0.517083	-1159.683298	0.099026	0.092741	-1159.782324	-1159.776038
	-1160.231968	0.51741	-1159.680056	0.099953	0.093183	-1159.780009	-1159.773239
	-1160.239085	0.516032	-1159.688023	0.099472	0.093727	-1159.787495	-1159.781751
	-1160.230786	0.516729	-1159.679097	0.099126	0.0935	-1159.778222	-1159.772596
BP86	-1160.799066	0.51454	-1160.249715	0.10024	0.093622	-1160.349955	-1160.343337
	-1160.795942	0.515043	-1160.246044	0.101121	0.094026	-1160.347165	-1160.34007
	-1160.787996	0.513661	-1160.239064	0.099597	0.094067	-1160.338661	-1160.333131
	-1160.779544	0.51422	-1160.230062	0.099715	0.094074	-1160.329778	-1160.324136
BP86 GD3BJ	-1160.954722	0.515719	-1160.404506	0.099081	0.09286	-1160.503587	-1160.497366
	-1160.951481	0.516859	-1160.400386	0.097638	0.092126	-1160.498025	-1160.492513
	-1160.954352	0.514536	-1160.404779	0.098504	0.093454	-1160.503283	-1160.498233
	-1160.945764	0.515558	-1160.395393	0.097906	0.093065	-1160.493299	-1160.488458
PBEPBE	-1159.395883	0.51637	-1158.844881	0.099572	0.093178	-1158.944453	-1158.938059
	-1159.392681	0.516773	-1158.841191	0.100346	0.093538	-1158.941536	-1158.934728
	-1159.384059	0.515311	-1158.833595	0.099344	0.09385	-1158.932939	-1158.927445
	-1159.375577	0.515934	-1158.82451	0.099543	0.09385	-1158.924053	-1158.91836
PBEPBE GD3BJ	-1159.448887	0.516976	-1158.897521	0.098509	0.092512	-1158.99603	-1158.990032
	-1159.486908	0.517582	-1158.934817	0.099231	0.092897	-1159.034047	-1159.027714
	-1159.484453	0.516115	-1158.933419	0.098262	0.093226	-1159.03168	-1159.026644
	-1159.47588	0.516459	-1158.924388	0.099201	0.093691	-1159.023589	-1159.018078
B3P86	-1164.558949	0.53135	-1163.993571	0.099297	0.092479	-1164.092868	-1164.08605

	-1164.554895	0.533521	-1163.987866	0.097329	0.091213	-1164.085195	-1164.079078
	-1164.552626	0.530541	-1163.987691	0.09786	0.092495	-1164.085552	-1164.080186
	-1164.543359	0.531104	-1163.977819	0.098398	0.092719	-1164.076217	-1164.070538
M06-HF	-1160.15111	0.539752	-1159.577292	0.10142	0.09357	-1159.678712	-1159.670862
	-1160.142014	0.540533	-1159.567502	0.099787	0.092842	-1159.667289	-1159.660344
	-1160.193192	0.538576	-1159.620048	0.098353	0.092913	-1159.718401	-1159.712961
	-1160.1819	0.5396	-1159.607907	0.097383	0.092465	-1159.70529	-1159.700373
M06-HF GD3	-1160.161753	0.539922	-1159.587849	0.099948	0.092811	-1159.687798	-1159.68066
	-1160.152634	0.540583	-1159.578081	0.099771	0.092799	-1159.677852	-1159.670879
	-1160.205048	0.538644	-1159.631854	0.098316	0.092868	-1159.73017	-1159.724722
	-1160.193738	0.539615	-1159.619721	0.097531	0.092501	-1159.717253	-1159.712222
TPSSH	-1160.669775	0.529379	-1160.106006	0.100162	0.093187	-1160.206168	-1160.199193
	-1160.666447	0.529913	-1160.102128	0.100378	0.093259	-1160.202506	-1160.195386
	-1160.662856	0.528319	-1160.09965	0.099137	0.093557	-1160.198787	-1160.193207
	-1160.654015	0.528931	-1160.090207	0.099577	0.093665	-1160.189784	-1160.183871
M11	-1159.940051	0.529662	-1159.376673	0.09845	0.09184	-1159.475123	-1159.468513
	-1159.935202	0.530298	-1159.371178	0.098568	0.091918	-1159.469746	-1159.463096
	-1159.95041	0.528579	-1159.387763	0.096205	0.091609	-1159.483968	-1159.479372
	-1159.940435	0.529978	-1159.3767	0.095239	0.090972	-1159.471939	-1159.467672
CAM-B3LYP	-1160.000902	0.536502	-1159.430798	0.098472	0.091692	-1159.52927	-1159.52249
	-1159.996856	0.537083	-1159.426157	0.099195	0.091997	-1159.525352	-1159.518154
	-1160.000423	0.535589	-1159.430839	0.096917	0.091741	-1159.527756	-1159.52258
	-1159.991109	0.536366	-1159.420807	0.096816	0.091628	-1159.517623	-1159.512436
CAM-B3LYP GD3BJ	-1160.08455	0.537288	-1159.513895	0.096916	0.090871	-1159.61081	-1159.604766
	-1160.080397	0.537679	-1159.509286	0.097346	0.0911	-1159.606633	-1159.600386
	-1160.090313	0.536217	-1159.520293	0.096018	0.091232	-1159.61631	-1159.611524
	-1160.080893	0.536633	-1159.510328	0.096988	0.091683	-1159.607316	-1159.602011

HF	-1152.727302	0.565532	-1152.129522	0.095657	0.089352	-1152.225179	-1152.218874
	-1152.716285	0.566307	-1152.117771	0.095507	0.089271	-1152.213277	-1152.207042
	-1152.777771	0.563308	-1152.18115	0.097007	0.0911	-1152.278157	-1152.27225
	-1152.764512	0.564443	-1152.166872	0.096688	0.090843	-1152.263561	-1152.257716
CAM-B3LYP GD3	**-1160.062339**	**0.537643**	**-1159.491503**	**0.096741**	**0.0906**	**-1159.588244**	**-1159.582104**
	-1160.058201	**0.538094**	**-1159.486891**	**0.096738**	**0.090626**	**-1159.583629**	**-1159.577517**
	-1160.068414	**0.536656**	**-1159.498162**	**0.095584**	**0.090778**	**-1159.593746**	**-1159.58894**
	-1160.059013	0.538154	-1159.487646	0.094184	0.089936	-1159.58183	-1159.577582
MPW1PW91	-1160.479218	0.534355	-1159.911024	0.09884	0.09211	-1160.009864	-1160.003134
	-1160.475001	0.534971	-1159.906181	0.099058	0.092144	-1160.005239	-1159.998325
	-1160.474114	0.533268	-1159.906526	0.097738	0.092408	-1160.004264	-1159.998934
	-1160.464607	0.533832	-1159.896409	0.098196	0.092582	-1159.994605	-1159.988992
PBE1PBE	-1159.44706	0.533321	-1158.879895	0.098732	0.092079	-1158.978628	-1158.971975
	-1159.442709	0.535407	-1158.873974	0.096509	0.090703	-1158.970483	-1158.964677
	-1159.441651	0.53232	-1158.875061	0.097519	0.092262	-1158.97258	-1158.967323
	-1159.432151	0.53284	-1158.86496	0.098238	0.092608	-1158.963198	-1158.957568
PBE1PBE GD3BJ	-1159.534164	0.534185	-1158.966398	0.097177	0.091222	-1159.063575	-1159.05762
	-1159.52985	0.534648	-1158.961553	0.097758	0.091494	-1159.059311	-1159.053047
	-1159.534753	0.533018	-1158.967673	0.09648	0.091697	-1159.064153	-1159.059371
	-1159.525192	0.533447	-1158.957574	0.097414	0.092157	-1159.054987	-1159.049731
BHandHLYP	-1159.75735	0.549061	-1159.175138	0.097948	0.091027	-1159.273086	-1159.266165
	-1159.75193	0.549834	-1159.169011	0.09757	0.090754	-1159.266581	-1159.259765
	-1159.76892	0.547911	-1159.187346	0.096621	0.091281	-1159.283967	-1159.278627
	-1159.758572	0.550122	-1159.175449	0.093897	0.089498	-1159.269346	-1159.264947
M06	-1159.938264	0.527005	-1159.377629	0.096922	0.091161	-1159.474551	-1159.46879
	-1159.934675	0.527504	-1159.373523	0.096978	0.091198	-1159.470501	-1159.464721
	-1159.937708	0.525954	-1159.377698	0.095759	0.091355	-1159.473458	-1159.469053

	-1159.928696	0.52648	-1159.368148	0.095725	0.09144	-1159.463873	-1159.459588
M06 GD3	-1159.954986	0.527206	-1159.394284	0.096101	0.090761	-1159.490385	-1159.485045
	-1159.951367	0.527426	-1159.390222	0.097495	0.091429	-1159.487717	-1159.481651
	-1159.956022	0.525957	-1159.396012	0.095705	0.091326	-1159.491717	-1159.487338
	-1159.946974	0.526479	-1159.386428	0.095646	0.091404	-1159.482074	-1159.477833
M06-2X	-1160.120889	0.534115	-1159.552972	0.098268	0.091852	-1159.65124	-1159.644823
	-1160.115929	0.534492	-1159.547472	0.099723	0.092556	-1159.647195	-1159.640028
	-1160.134132	0.53278	-1159.567002	0.097766	0.092434	-1159.664768	-1159.659436
	-1160.124476	0.534095	-1159.556298	0.096889	0.091844	-1159.653187	-1159.648142
M06-2X GD3	-1160.127133	0.534119	-1159.559209	0.098255	0.091839	-1159.657464	-1159.651049
	-1160.122164	0.534501	-1159.553718	0.099495	0.092474	-1159.653214	-1159.646192
	-1160.140958	0.532627	-1159.574821	0.094952	0.090483	-1159.669773	-1159.665304
	-1160.131298	0.534149	-1159.563088	0.096766	0.091766	-1159.659853	-1159.654853

Table 8. Experimental and Expected ΔG values of Benzonitrile Nickel Complexes in THF and Toluene with correction.

*Best performing methods are **bolded**. ΔG consistent with theoretical ΔG sign (+/-) and within the experimental **2.1-2.5** range are considered best performing functionals. All ΔG units measured in (kcal/mol)

Method	**E/au**	**G**	**qh-G**	**ΔG**	**qh-ΔG**	Validity	**ΔGexpt**
SVWN	-1155.8516	-1155.4004	-1155.3941	5.76	4.65	x	-1.16
	-1155.8474	-1155.3957	-1155.3892	9.27	8.07	x	-0.51
	-1155.8441	-1155.3912	-1155.3867	0.62	0.58		2.3
	-1155.8342	-1155.3809	-1155.3763				
M06L	-1160.804	-1160.3388	-1160.3324	-0.56	-1.21		-1.16
	-1160.8008	-1160.3348	-1160.3285	3.81	3.01	x	-0.51
	-1160.8044	-1160.3397	-1160.3343	-0.15	-0.40		2.3
	-1160.7951	-1160.3287	-1160.3237				
M06L GD3	-1160.8111	-1160.3467	-1160.3399	-0.22	-1.23		-1.16
	-1160.8079	-1160.3428	-1160.336	4.07	2.95	x	-0.51
	-1160.8121	-1160.3471	-1160.3418	-0.05	-0.42		2.3
	-1160.8028	-1160.3363	-1160.3313				
M11L	-1160.9532	-1160.4946	-1160.4888	-0.04	-1.02		-1.16
	-1160.9495	-1160.4908	-1160.4847	3.74	2.71	x	-0.51
	-1160.9545	-1160.4946	-1160.4904	-0.01	-0.38		2.3
	-1160.9448	-1160.4848	-1160.4804				
TPSSTPSS	-1161.0185	-1160.5612	-1160.5543	2.97	2.20	x	-1.16
	-1161.0152	-1160.5576	-1160.5506	6.84	6.15	x	-0.51
	-1161.014	-1160.5565	-1160.5508	0.43	0.36		2.3
	-1161.0045	-1160.5467	-1160.5408				
TPSSTPSS GD3BJ	-1161.1394	-1160.6806	-1160.674	-1.80	-2.76		-1.16
	-1161.136	-1160.6768	-1160.6702	2.19	1.29	x	-0.51
	-1161.143	-1160.6835	-1160.6784	-0.82	-2.14		2.3

	-1161.1334	-1160.6734	-1160.6681				
B3LYP	-1160.9089	-1160.4437	-1160.4368	-0.99	-1.95		-1.16
	-1160.9047	-1160.4388	-1160.432	2.90	1.98	x	-0.51
	-1160.9114	-1160.4452	-1160.4399	-0.34	-0.99		2.3
	-1160.901	-1160.4342	-1160.4288				
B3LYP GD3BJ	**-1161.068**	**-1160.5999**	**-1160.5938**	**-8.26**	**-8.71**		**-1.16**
	-1161.0636	**-1160.5952**	**-1160.589**	**-3.61**	**-4.29**		**-0.51**
	-1161.0802	**-1160.6131**	**-1160.6077**	**2.29**	**2.03**		**2.3**
	-1161.0696	-1160.601	-1160.5958				
B3PW91	-1160.6123	-1160.1462	-1160.1395	1.64	0.81	x	-1.16
	-1160.608	-1160.1415	-1160.1347	5.61	4.70	x	-0.51
	-1160.61	-1160.1436	-1160.1382	0.29	0.17		2.3
	-1160.5997	-1160.1326	-1160.1272				
B3PW91 GD3BJ	-1160.779	-1160.3102	-1160.3042	-5.69	-6.33		-1.16
	-1160.7745	-1160.3053	-1160.2991	-0.17	-1.51		-0.51
	-1160.7872	-1160.3193	-1160.3143	34.34	4.19	x	2.3
	-1160.7768	-1160.3056	-1160.3016				
B3LYP GD3	**-1160.9955**	**-1160.527**	**-1160.5211**	**-7.01**	**-7.72**		**-1.16**
	-1160.9911	**-1160.5228**	**-1160.5166**	**-2.19**	**-3.20**		**-0.51**
	-1161.0071	**-1160.5382**	**-1160.5334**	**3.20**	**2.42**		**2.3**
	-1160.9966	-1160.5263	-1160.5216				
B97D	-1160.7219	-1160.2698	-1160.2635	-2.42	-3.18		-1.16
	-1160.7182	-1160.2639	-1160.2579	1.76	0.81	x	-0.51
	-1160.7264	-1160.2737	-1160.2685	-1.37	-3.95		2.3
	-1160.7163	-1160.2611	-1160.2566				
B97D3	-1160.8172	-1160.3604	-1160.3541	-1.60	-2.37		-1.16
	-1160.8137	-1160.3567	-1160.3503	1.98	1.49	x	-0.51
	-1160.8204	-1160.363	-1160.3579	-0.81	-1.59		2.3

	-1160.8104	-1160.3535	-1160.3479				
	-1160.3179	-1159.8684	-1159.8616	1.88	1.17	x	-1.16
BLYP	-1160.3146	-1159.865	-1159.858	6.23	5.34	x	-0.51
	-1160.3154	-1159.8654	-1159.8598	0.30	0.22		2.3
	-1160.3056	-1159.8551	-1159.8495				
BLYP GD3BJ	-1160.5079	-1160.0554	-1160.0491	-6.25	-6.59		-1.16
	-1160.5043	-1160.0523	-1160.0456	-1.32	-2.04		-0.51
	-1160.517	-1160.0654	-1160.0596	4.74	3.24	x	2.3
	-1160.507	-1160.0544	-1160.0488				
BP86	-1161.0461	-1160.597	-1160.5904	4.10	3.42	x	-1.16
	-1161.0425	-1160.5937	-1160.5867	8.43	7.52	x	-0.51
	-1161.0398	-1160.5904	-1160.5849	0.49	0.45		2.3
	-1161.0301	-1160.5803	-1160.5747				
BP86 GD3BJ	-1161.2018	-1160.7507	-1160.7444	-2.62	-3.35		-1.16
	-1161.1981	-1160.7446	-1160.7391	0.61	0.19	x	-0.51
	-1161.2059	-1160.7548	-1160.7498	-4.26	-17.35		2.3
	-1161.1961	-1160.7436	-1160.7388				
PBEPBE	-1159.6353	-1159.1839	-1159.1775	4.33	3.77	x	-1.16
	-1159.6317	-1159.1806	-1159.1738	8.59	7.89	x	-0.51
	-1159.6281	-1159.177	-1159.1715	0.50	0.48		2.3
	-1159.6184	-1159.1669	-1159.1612				
PBEPBE GD3BJ	-1159.6883	-1159.2354	-1159.2294	-25.18	-25.78		-1.16
	-1159.7259	-1159.273	-1159.2667	4.27	3.75	x	-0.51
	-1159.7283	-1159.2755	-1159.2705	-5.90	-6.87		2.3
	-1159.7185	-1159.2662	-1159.2607				
B3P86	-1164.7854	-1164.3193	-1164.3125	1.67	0.76	x	-1.16
	-1164.7809	-1164.3112	-1164.3051	3.09	2.82	x	-0.51
	-1164.7837	-1164.3167	-1164.3113	0.54	0.27		2.3

	-1164.7734	-1164.3063	-1164.3006				
M06-HF	-1160.4156	-1159.9432	-1159.9354	-30.23	-31.74		-1.16
	-1160.4051	-1159.9304	-1159.9234	-28.94	-30.21		-0.51
	-1160.4662	-1159.9914	-1159.986	1.04	1.05	x	2.3
	-1160.4531	-1159.9765	-1159.9716				
M06-HF GD3	-1160.4263	-1159.9523	-1159.9452	-31.91	-32.97		-1.16
	-1160.4158	-1159.941	-1159.934	-29.77	-30.99		-0.51
	-1160.4781	-1160.0032	-1159.9977	1.07	1.06	x	2.3
	-1160.4649	-1159.9884	-1159.9834				
TPSSH	-1160.8909	-1160.4273	-1160.4204	1.75	0.88	x	-1.16
	-1160.8873	-1160.4233	-1160.4162	5.52	4.76	x	-0.51
	-1160.8886	-1160.4245	-1160.419	0.32	0.18		2.3
	-1160.8788	-1160.4145	-1160.4086				
M11	-1160.1922	-1159.7272	-1159.7206	-11.05	-12.32		-1.16
	-1160.1865	-1159.721	-1159.7144	-6.59	-8.08		-0.51
	-1160.2113	-1159.7448	-1159.7402	1.68	1.52	x	2.3
	-1160.2	-1159.7315	-1159.7273				
CAM-B3LYP	-1160.2481	-1159.7764	-1159.7696	-2.75	-3.75		-1.16
	-1160.2432	-1159.7717	-1159.7645	1.59	0.33	x	-0.51
	-1160.2535	-1159.7808	-1159.7756	-1.72	-11.29		2.3
	-1160.2427	-1159.7692	-1159.764				
CAM-B3LYP GD3BJ	-1160.3317	-1159.8579	-1159.8519	-7.10	-7.89		-1.16
	-1160.3267	-1159.853	-1159.8467	-3.63	-4.22		-0.51
	-1160.3432	-1159.8692	-1159.8644	1.95	1.87	x	2.3
	-1160.3323	-1159.8588	-1159.8534				
HF	-1152.9195	-1152.4173	-1152.411	-35.85	-36.10		-1.16
	-1152.9078	-1152.4048	-1152.3985	-34.04	-34.28		-0.51
	-1152.9741	-1152.4745	-1152.4686	1.05	1.05	x	2.3

	-1152.96	-1152.459	-1152.4532				
CAM-B3LYP GD3	**-1160.3094**	**-1159.8353**	**-1159.8292**	**-7.06**	**-7.89**		**-1.16**
	-1160.3045	**-1159.8299**	**-1159.8238**	**-2.03**	**-3.20**		**-0.51**
	-1160.3212	**-1159.8465**	**-1159.8417**	**3.47**	**2.46**		**2.3**
	-1160.3103	-1159.8332	-1159.8289				
MPW1PW91	-1160.6975	-1160.2281	-1160.2214	0.62	-0.25		-1.16
	-1160.6928	-1160.2231	-1160.2162	4.13	3.31	x	-0.51
	-1160.697	-1160.2271	-1160.2218	0.15	-0.08		2.3
	-1160.6865	-1160.2165	-1160.2109				
PBE1PBE	-1159.6617	-1159.1932	-1159.1866	1.00	0.13	x	-1.16
	-1159.6569	-1159.1846	-1159.1788	2.14	2.03	x	-0.51
	-1159.6607	-1159.1916	-1159.1864	0.47	0.06		2.3
	-1159.6502	-1159.1812	-1159.1756				
PBE1PBE GD3BJ	-1159.7488	-1159.2782	-1159.2723	-3.06	-3.80		-1.16
	-1159.744	-1159.2735	-1159.2672	0.33	-0.30		-0.51
	-1159.7537	-1159.2831	-1159.2783	-9.23	12.65	x	2.3
	-1159.7432	-1159.273	-1159.2677				
BHandHLYP	-1159.9729	-1159.4886	-1159.4817	-9.94	-10.93		-1.16
	-1159.9669	-1159.4815	-1159.4747	-4.48	-5.99		-0.51
	-1159.9894	-1159.5045	-1159.4991	2.22	1.82	x	2.3
	-1159.9779	-1159.4887	-1159.4843				
M06	-1160.1734	-1159.7097	-1159.704	-2.22	-3.07		-1.16
	-1160.1696	-1159.7054	-1159.6996	1.63	0.69	x	-0.51
	-1160.1775	-1159.7133	-1159.7089	-1.36	-4.45		2.3
	-1160.1676	-1159.7028	-1159.6985				
M06 GD3	-1160.1902	-1159.7256	-1159.7202	-3.72	-4.32		-1.16
	-1160.1863	-1159.7226	-1159.7166	1.03	-0.11		-0.51
	-1160.1958	-1159.7315	-1159.7271	-3.60	37.82	x	2.3

	-1160.1859	-1159.721	-1159.7168				
M06-2X	-1160.3721	-1159.9024	-1159.896	-12.04	-12.72		-1.16
	-1160.3663	-1159.8975	-1159.8904	-7.00	-8.33		-0.51
	-1160.391	-1159.9216	-1159.9163	1.72	1.53	x	2.3
	-1160.38	-1159.9087	-1159.9036				
M06-2X GD3	-1160.3783	-1159.9087	-1159.9023	-11.27	-12.49		-1.16
	-1160.3725	-1159.9036	-1159.8965	-7.40	-8.67		-0.51
	-1160.3978	-1159.9266	-1159.9222	1.52	1.44	x	2.3
	-1160.3868	-1159.9154	-1159.9104				

Table 9. Solvation Energies and Thermochemical Corrections for C—CN Bond Activation of Fluorinated Benzonitriles.

	E/au	ZPE/au	H/au	T.S/au	G(T)/au	spe(tol)	spe(thf)
S1-26F2	-945.36116	0.294392	-945.04269	0.077014	-945.11971	-945.5843	-945.58999
S1-2F1	-846.12863	0.30237	-845.8029	0.076456	-845.87935	-846.31954	-846.32566
S1-2F2	-846.13318	0.302691	-845.80732	0.074816	-845.88213	-846.32053	-846.32526
S1-35F2	-945.36141	0.294112	-945.04308	0.078526	-945.12161	-945.58985	-945.59513
S1-3F1	-846.13103	0.302351	-845.80533	0.076439	-845.88176	-846.32288	-846.3281
S1-3F2	-846.13056	0.302331	-845.80487	0.076512	-845.88139	-846.32255	-846.32794
S1-4F	-846.13111	0.302375	-845.80538	0.076372	-845.88175	-846.32287	-846.32823
S1-H	-746.89931	0.310543	-746.56624	0.074391	-746.64063	-747.05409	-747.05926
S5-26F2	-945.36878	0.292987	-945.05091	0.078607	-945.12951	-945.60361	-945.61511
S5-2F1	-846.13027	0.301083	-845.80519	0.076439	-845.88163	-846.32958	-846.3404
S5-2F2	-846.1302	0.301222	-845.80506	0.076137	-845.8812	-846.32897	-846.33974
S5-35F2	-945.3557	0.292851	-945.03801	0.078604	-945.11662	-945.59481	-945.60626
S5-3F1	-846.12326	0.301015	-845.79827	0.076544	-845.87482	-846.3251	-846.33627
S5-3F2	-846.12326	0.301021	-845.79827	0.076509	-845.87478	-846.32511	-846.3363
S5-4F	-846.12171	0.301016	-845.79671	0.076624	-845.87334	-846.3233	-846.33446
S5-H	-746.88986	0.309152	-746.55757	0.074438	-746.63201	-747.05385	-747.06464
TS25-26F2	-945.31426	0.291457	-944.99841	0.07732	-945.07573	-945.53786	-945.54329
TS25-2F1	-846.08601	0.299587	-845.76296	0.075343	-845.8383	-846.27767	-846.28397
TS25-2F2	-846.08168	0.299363	-845.75864	0.076522	-845.83516	-846.27317	-846.2791
TS25-35F2	-945.3142	0.291055	-944.99874	0.078066	-945.07681	-945.54578	-945.55204
TS25-3F1	-846.08366	0.299322	-845.7608	0.076037	-845.83684	-846.27883	-846.28521
TS25-3F2	-846.0835	0.299308	-845.76065	0.076095	-845.83674	-846.27865	-846.28501
TS25-4F	-846.08346	0.29946	-845.76049	0.076015	-845.8365	-846.27859	-846.28521
TS25-H	-746.85207	0.307545	-746.52182	0.074086	-746.5959	-747.01019	-747.01652

Table 10. ΔG Calculated for C—CN Bond Activation of Fluorinated Benzonitriles.

	E/au	G(T)/au	spe(tol)	spe(thf)	G(tol)	G(thf)	ΔG(tol)	ΔG(thf)
S1-26F2	-945.36116	-945.11971	-945.5843	-945.58999	-945.34285	-945.34853	0.0	0.0
S1-2F1	-846.12863	-845.87935	-846.31954	-846.32566	-846.07027	-846.07638	0.0	0.0
S1-2F2	-846.13318	-845.88213	-846.32053	-846.32526	-846.06948	-846.07422	0.5	1.4
S1-35F2	-945.36141	-945.12161	-945.58985	-945.59513	-945.35005	-945.35532	0.0	0.0
S1-3F1	-846.13103	-845.88176	-846.32288	-846.3281	-846.07361	-846.07883	0.0	0.0
S1-3F2	-846.13056	-845.88139	-846.32255	-846.32794	-846.07337	-846.07876	0.1	0.0
S1-4F	-846.13111	-845.88175	-846.32287	-846.32823	-846.07351	-846.07887	0.0	0.0
S1-H	-746.89931	-746.64063	-747.05409	-747.05926	-746.79541	-746.80058	0.0	0.0
S5-26F2	-945.36878	-945.12951	-945.60361	-945.61511	-945.36435	-945.37585	-13.5	-17.1
S5-2F1	-846.13027	-845.88163	-846.32958	-846.3404	-846.08094	-846.09176	-6.7	-9.7
S5-2F2	-846.1302	-845.8812	-846.32897	-846.33974	-846.07997	-846.09074	-6.1	-9.0
S5-35F2	-945.3557	-945.11662	-945.59481	-945.60626	-945.35573	-945.36718	-3.6	-7.4
S5-3F1	-846.12326	-845.87482	-846.3251	-846.33627	-846.07665	-846.08783	-1.9	-5.6
S5-3F2	-846.12326	-845.87478	-846.32511	-846.3363	-846.07663	-846.08782	-1.9	-5.6
S5-4F	-846.12171	-845.87334	-846.3233	-846.33446	-846.07492	-846.08608	-0.9	-4.5
S5-H	-746.88986	-746.63201	-747.05385	-747.06464	-746.796	-746.80679	-0.4	-3.9
TS25-26F2	-945.31426	-945.07573	-945.53786	-945.54329	-945.29934	-945.30477	27.3	27.5
TS25-2F1	-846.08601	-845.8383	-846.27767	-846.28397	-846.02996	-846.03626	25.3	25.2
TS25-2F2	-846.08168	-845.83516	-846.27317	-846.2791	-846.02666	-846.03259	27.4	27.5
TS25-35F2	-945.3142	-945.07681	-945.54578	-945.55204	-945.30839	-945.31465	26.1	25.5
TS25-3F1	-846.08366	-845.83684	-846.27883	-846.28521	-846.03201	-846.0384	26.1	25.4
TS25-3F2	-846.0835	-845.83674	-846.27865	-846.28501	-846.03189	-846.03825	26.2	25.5
TS25-4F	-846.08346	-845.8365	-846.27859	-846.28521	-846.03163	-846.03826	26.3	25.5
TS25-H	-746.85207	-746.5959	-747.01019	-747.01652	-746.75402	-746.76035	26.0	25.2

Future work

From the data obtained with the [Ni(dmpe)] ligand and the benchmarking study, our research group would like to take what we have learned from these studies and apply it to a full ligand DFT analysis using [Ni(dippe)]. DFT calculations with the [Ni(dippe)] fragment with a C2 symmetric ligand are currently underway. It is important to state that there has been some difficulty in finding the transition states while employing the [Ni(dippe)] ligands due to ligand-substrate interactions.

CHAPTER V

CONCLUSIONS

Due to the high polarity of the C—CN bond cleavage products, solvent effects were taken into consideration in all DFT calculations in terms of the SMD correction, and the results show excellent agreement with the experimental observations. Both experimental and DFT calculation results for the reaction of $[Ni(dmpe)H]_2$ with benzonitriles revealed that the number of ortho-F substituents affects the product stability. After investigating the 2-F, 3-F, 4-F, 2,6-F2, and 3,5-F2benzonitrile substrates, results have shown that there is a very good correlation between the stability of the C—CN bond activation products and the number of o-fluoro substituents. Although the C—C bond activation barrier is relatively constant with a slightly higher barrier for 2,6-F2 substrate due to steric hindrance, the activation barriers for the C—C bond elimination show a good correlation with the number of o-F substituents. For the future work, we will continue the DFT analysis with [Ni(dippe)] using the results from our benchmarking study.

REFERENCES

1. Halpern, Jack. "Determination and Significance of Transition Metal-Alkyl Bond Dissociation Energies." *Accounts of Chemical Research* 15, no. 8 (1982): 238–44. https://doi.org/10.1021/ar00080a002.
2. Crabtree, Robert H., Elizabeth M. Holt, Maryellen Lavin, and Sheila M. Morehouse. "Inter- vs. Intramolecular Carbon-Hydrogen Activation: A Carbon-Hydrogen-Iridium Bridge in [IrH2(Mq)L2]BF4 and a CH + M .Fwdarw. CMH Reaction Trajectory." *Inorganic Chemistry* 24, no. 13 (1985): 1986–92. https://doi.org/10.1021/ic00207a008.
3. Souillart, Laetitia, and Nicolai Cramer. "Catalytic C–C Bond Activations via Oxidative Addition to Transition Metals." *Chemical Reviews* 115, no. 17 (2015): 9410–64. https://doi.org/10.1021/acs.chemrev.5b00138.
4. Cramer, Nicolai, and Tobias Seiser. "β-Carbon Elimination from Cyclobutanols. A Clean Access to Alkylrhodium Intermediates Bearing a Quaternary Stereogenic Center." *Synlett* 2011, no. 4 (2011): 449–60. https://doi.org/10.1055/s-0030-1259536.
5. Rodríguez, Nuria, and Lukas J. Goossen. "Decarboxylative Coupling Reactions: A Modern Strategy for C–C-Bond Formation." *Chem. Soc. Rev.* 40, no. 10 (2011): 5030–48. https://doi.org/10.1039/C1CS15093F.
6. Taw, Felicia L., Peter S. White, Robert G. Bergman, and Maurice Brookhart. "Carbon−Carbon Bond Activation of R−CN (R = Me, Ar, IPr, TBu) Using a Cationic Rh(III)

Complex." *Journal of the American Chemical Society* 124, no. 16 (2002): 4192–93. https://doi.org/10.1021/ja0255094.

7. Nakazawa, Hiroshi, Kouji Kamata, and Masumi Itazaki. "Catalytic C–C Bond Cleavage and C–Si Bond Formation in the Reaction of RCN with Et3SiH Promoted by an Iron Complex." *Chem. Commun.*, no. 31 (2005): 4004–6. https://doi.org/10.1039/B504131G.
8. Muetterties, E. L., D. H. Gerlach, A. R. Kane, G. W. Parshall, and J. P. Jesson. "Reactivity of Trialkylphosphine Complexes of Platinum(0)." *Journal of the American Chemical Society* 93, no. 14 (1971): 3543–44. https://doi.org/10.1021/ja00743a050.
9. Seidel, W. C., and C. A. Tolman. "HOMOGENEOUS NICKEL-CATALYZED OLEFIN HYDROCYANATION." *Annals of the New York Academy of Sciences* 415, no. 1 (1983): 201–201. https://doi.org/10.1111/j.1749-6632.1983.tb47360.x.
10. Garcia, Juventino J., and William D. Jones. "Reversible Cleavage of Carbon−Carbon Bonds in Benzonitrile Using Nickel(0)." *Organometallics* 19, no. 26 (2000): 5544–45. https://doi.org/10.1021/om0008474.
11. Garcia, Juventino J., Nicole M. Brunkan, and William D. Jones. "Cleavage of Carbon−Carbon Bonds in Aromatic Nitriles Using Nickel(0)." *Journal of the American Chemical Society* 124, no. 32 (2002): 9547–55. https://doi.org/10.1021/ja0204933.
12. Ateşin, Tülay A., Ting Li, Sébastien Lachaize, Juventino J. García, and William D. Jones. "Experimental and Theoretical Examination of C−CN Bond Activation of Benzonitrile Using Zerovalent Nickel." *Organometallics* 27, no. 15 (2008): 3811–17. https://doi.org/10.1021/om800424s.
13. Li, Ting, Juventino J. García, William W. Brennessel, and William D. Jones. "C−CN Bond Activation of Aromatic Nitriles and Fluxionality of the H2-Arene Intermediates:

Experimental and Theoretical Investigations." *Organometallics* 29, no. 11 (2010): 2430–45. https://doi.org/10.1021/om100001m.

14. García, Juventino J., Alma Arévalo, Nicole M. Brunkan, and William D. Jones. "Cleavage of Carbon−Carbon Bonds in Alkyl Cyanides Using Nickel(0)." *Organometallics* 23, no. 16 (2004): 3997–4002. https://doi.org/10.1021/om049700t.
15. Ateşin, Tülay A., Ting Li, Sébastien Lachaize, William W. Brennessel, Juventino J. García, and William D. Jones. "Experimental and Theoretical Examination of C−CN and C−H Bond Activations of Acetonitrile Using Zerovalent Nickel." *Journal of the American Chemical Society* 129, no. 24 (2007): 7562–69. https://doi.org/10.1021/ja0707153.
16. Brunkan, Nicole M., Donna M. Brestensky, and William D. Jones. "Kinetics, Thermodynamics, and Effect of BPh3 on Competitive C−C and C−H Bond Activation Reactions in the Interconversion of Allyl Cyanide by [Ni(Dippe)]." *Journal of the American Chemical Society* 126, no. 11 (2004): 3627–41. https://doi.org/10.1021/ja037002e.
17. Swartz, Brett D., Nicole M. Reinartz, William W. Brennessel, Juventino J. García, and William D. Jones. "Solvent Effects and Activation Parameters in the Competitive Cleavage of C−CN and C−H Bonds in 2-Methyl-3-Butenenitrile Using [(Dippe)NiH]2." *Journal of the American Chemical Society* 130, no. 26 (2008): 8548–54. https://doi.org/10.1021/ja8000216.
18. Li, Ting, and William D. Jones. "DFT Calculations of the Isomerization of 2-Methyl-3-Butenenitrile by [Ni(Bisphosphine)] in Relation to the DuPont Adiponitrile Process." *Organometallics* 30, no. 3 (2011): 547–55. https://doi.org/10.1021/om100907y.
19. Grochowski, Matthew R., Ting Li, William W. Brennessel, and William D. Jones. "Competitive Carbon−Sulfur vs Carbon−Carbon Bond Activation of 2-Cyanothiophene with

[Ni(Dippe)H]$_2$." *Journal of the American Chemical Society* 132, no. 35 (2010): 12412–21. https://doi.org/10.1021/ja104158h.

20. Acosta-Ramírez, Alberto, Miguel Muñoz-Hernández, William D. Jones, and Juventino J. García. "Catalytic Isomerization of 2-Methyl-3-Butenenitrile by Nickel Systems Using Bis-Diphosphinoferrocene Ligands: Evidence for Hemilability." *Organometallics* 26, no. 24 (2007): 5766–69. https://doi.org/10.1021/om700928y.
21. Swartz, B. D.; Brennessel, W. W.; Jones, W. D., "Lewis Acid Assisted C-CN Cleavage of Benzonitrile Using [(dippe)NiH]$_2$." *Synlett* 29, no. 6 (2018): 747-753. https://doi.org/10.1055/s-0036-1590801.
22. Camasso, Nicole M., and Melanie S. Sanford. "Design, Synthesis, and Carbon-Heteroatom Coupling Reactions of Organometallic Nickel(IV) Complexes." *Science* 347, no. 6227 (2015): 1218–20. https://doi.org/10.1126/science.aaa4526.
23. Zhang, Heng, and Aiwen Lei. "Palladium(Iv) Chemistry Supported by Pincer Type Ligands." *Dalton Trans.* 40, no. 35 (2011): 8745–54. https://doi.org/10.1039/C1DT10373C.
24. Zheng, Chao, and Shu-Li You. "Recent Development of Direct Asymmetric Functionalization of Inert C–H Bonds." *RSC Adv.* 4, no. 12 (2014): 6173–6214. https://doi.org/10.1039/C3RA46996D.
25. Zhao, Yan, Hou T. Ng, Roberto Peverati, and Donald G. Truhlar. "Benchmark Database for Ylidic Bond Dissociation Energies and Its Use for Assessments of Electronic Structure Methods." *Journal of Chemical Theory and Computation* 8, no. 8 (2012): 2824–34. https://doi.org/10.1021/ct300457c.

26. Sieffert, Nicolas, and Michael Bühl. “Noncovalent Interactions in a Transition-Metal Triphenylphosphine Complex: A Density Functional Case Study.” *Inorganic Chemistry* 48, no. 11 (2009): 4622–24. https://doi.org/10.1021/ic900347e.

27. Sparta, Manuel, Vidar R. Jensen, and Knut J. Børve. “Accurate Metal–Ligand Bond Energies in the H2-C2H4 and H2-C60 Complexes of Pt(PH3)2, with Application to Their Bis(Triphenylphosphine) Analogues.” *Molecular Physics* 111, no. 9–11 (2013): 1599–1611. https://doi.org/10.1080/00268976.2013.809489.

28. Grimme, Stefan. “Semiempirical GGA-Type Density Functional Constructed with a Long-Range Dispersion Correction.” *Journal of Computational Chemistry* 27, no. 15 (2006): 1787–99. https://doi.org/10.1002/jcc.20495.

29. Grimme, Stefan, Jens Antony, Stephan Ehrlich, and Helge Krieg. “A Consistent and Accurate Ab Initio Parametrization of Density Functional Dispersion Correction (DFT-D) for the 94 Elements H-Pu.” *The Journal of Chemical Physics* 132, no. 15 (2010): 154104. https://doi.org/10.1063/1.3382344.

30. Grimme, Stefan, Stephan Ehrlich, and Lars Goerigk. “Effect of the Damping Function in Dispersion Corrected Density Functional Theory.” *Journal of Computational Chemistry* 32, no. 7 (2011): 1456–65. https://doi.org/10.1002/jcc.21759.

31. Cramer, Christopher J., and Donald G. Truhlar. “Density Functional Theory for Transition Metals and Transition Metal Chemistry.” *Phys. Chem. Chem. Phys.* 11, no. 46 (2009): 10757–816. https://doi.org/10.1039/B907148B.

32. Harvey, Jeremy N. “On the Accuracy of Density Functional Theory in Transition Metal Chemistry.” *Annu. Rep. Prog. Chem., Sect. C: Phys. Chem.* 102, no. 0 (2006): 203–26. https://doi.org/10.1039/B419105F.

33. Becke, Axel D. “Perspective: Fifty Years of Density-Functional Theory in Chemical Physics.” *The Journal of Chemical Physics* 140, no. 18 (2014): 18A301. https://doi.org/10.1063/1.4869598.

34. Born, M., and R. Oppenheimer. “Zur Quantentheorie Der Molekeln.” [On the Quantum Theory of Molecules]. *Annalen der Physik* (in German). 389, no. 20 (1927): 457–84. https://doi.org/10.1002/andp.19273892002.

35. Amusia, M. Ya, A. Z. Msezane, and V. R. Shaginyan. “Density Functional Theory versus the Hartree–Fock Method: Comparative Assessment.” *Physica Scripta* 68, no. 6 (January 2003): C133–40. https://doi.org/10.1238/physica.regular.068ac0133.

36. Yu, Haoyu S., Shaohong L. Li, and Donald G. Truhlar. “Perspective: Kohn-Sham Density Functional Theory Descending a Staircase.” *The Journal of Chemical Physics* 145, no. 13 (2016): 130901. https://doi.org/10.1063/1.4963168.

37. Rappoport, Dmitrij, N. Crawford, F. Furche, and K. Burke. “Which Functional Should I Choose,” 2009.

38. Kohn, W., and L. J. Sham. “Self-Consistent Equations Including Exchange and Correlation Effects.” *Phys. Rev.* 140, no. 4A (November 1965): A1133–38. https://doi.org/10.1103/PhysRev.140.A1133.

39. Hopmann, Kathrin H. “How Accurate Is DFT for Iridium-Mediated Chemistry?” *Organometallics* 35, no. 22 (2016): 3795–3807. https://doi.org/10.1021/acs.organomet.6b00377.

40. Sperger, Theresa, Italo A. Sanhueza, Indrek Kalvet, and Franziska Schoenebeck. “Computational Studies of Synthetically Relevant Homogeneous Organometallic Catalysis Involving Ni, Pd, Ir, and Rh: An Overview of Commonly Employed DFT Methods and

Mechanistic Insights." *Chemical Reviews* 115, no. 17 (2015): 9532–86. https://doi.org/10.1021/acs.chemrev.5b00163.

41. Orsino, Alessio F., Manuel Gutiérrez del Campo, Martin Lutz, and Marc-Etienne Moret. "Enhanced Catalytic Activity of Nickel Complexes of an Adaptive Diphosphine–Benzophenone Ligand in Alkyne Cyclotrimerization." *ACS Catalysis* 9, no. 3 (2019): 2458–81. https://doi.org/10.1021/acscatal.8b05025.
42. Wang, Jing, Mei-Yan Wang, Guoyin Yin, Ran Jia, Jian Wang, Roberts I. Eglitis, and Hong-Xing Zhang. "Nickel-Catalyzed Carboxylation of Aryl Zinc Reagent with CO2: A Theoretical and Experimental Study." *Journal of CO2 Utilization* 29 (2019): 262–70. https://doi.org/10.1016/j.jcou.2018.12.007.
43. Lin, You-Sheng, Chen-Wei Tsai, Guan-De Li, and Jeng-Da Chai. "Long-Range Corrected Hybrid Meta-Generalized-Gradient Approximations with Dispersion Corrections." *The Journal of Chemical Physics* 136, no. 15 (2012): 154109. https://doi.org/10.1063/1.4704370.
44. Grimme, Stefan, Andreas Hansen, Jan Gerit Brandenburg, and Christoph Bannwarth. "Dispersion-Corrected Mean-Field Electronic Structure Methods." *Chemical Reviews* 116, no. 9 (2016): 5105–54. https://doi.org/10.1021/acs.chemrev.5b00533.
45. Perdew, John P., and Karla Schmidt. "Jacob's Ladder of Density Functional Approximations for the Exchange-Correlation Energy." *AIP Conference Proceedings* 577, no. 1 (2001): 1–20. https://doi.org/10.1063/1.1390175.
46. Slater, J. C. "A Simplification of the Hartree-Fock Method." *Phys. Rev.* 81, no. 3 (February 1951): 385–90. https://doi.org/10.1103/PhysRev.81.385.

47. Vosko, S. H., L. Wilk, and M. Nusair. “Accurate Spin-Dependent Electron Liquid Correlation Energies for Local Spin Density Calculations: A Critical Analysis.” *Canadian Journal of Physics* 58, no. 8 (1980): 1200–1211. https://doi.org/10.1139/p80-159.

48. Staroverov, Viktor N., Gustavo E. Scuseria, Jianmin Tao, and John P. Perdew. “Comparative Assessment of a New Nonempirical Density Functional: Molecules and Hydrogen-Bonded Complexes.” *The Journal of Chemical Physics* 119, no. 23 (2003): 12129–37. https://doi.org/10.1063/1.1626543.

49. Perdew, John P., Kieron Burke, and Matthias Ernzerhof. “Generalized Gradient Approximation Made Simple.” *Phys. Rev. Lett.* 77, no. 18 (October 1996): 3865–68. https://doi.org/10.1103/PhysRevLett.77.3865.

50. Becke, A. D. “Density-Functional Exchange-Energy Approximation with Correct Asymptotic Behavior.” *Phys. Rev. A* 38, no. 6 (September 1988): 3098–3100. https://doi.org/10.1103/PhysRevA.38.3098.

51. Lee, Chengteh, Weitao Yang, and Robert G. Parr. “Development of the Colle-Salvetti Correlation-Energy Formula into a Functional of the Electron Density.” *Phys. Rev. B* 37, no. 2 (January 1988): 785–89. https://doi.org/10.1103/PhysRevB.37.785.

52. Tao, Jianmin, John P. Perdew, Viktor N. Staroverov, and Gustavo E. Scuseria. “Climbing the Density Functional Ladder: Nonempirical Meta–Generalized Gradient Approximation Designed for Molecules and Solids.” *Phys. Rev. Lett.* 91, no. 14 (September 2003): 146401. https://doi.org/10.1103/PhysRevLett.91.146401.

53. Zhao, Yan, and Donald G. Truhlar. “A New Local Density Functional for Main-Group Thermochemistry, Transition Metal Bonding, Thermochemical Kinetics, and Noncovalent

Interactions." *The Journal of Chemical Physics* 125, no. 19 (2006): 194101. https://doi.org/10.1063/1.2370993.

54. Peverati, Roberto, and Donald G. Truhlar. "M11-L: A Local Density Functional That Provides Improved Accuracy for Electronic Structure Calculations in Chemistry and Physics." *The Journal of Physical Chemistry Letters* 3, no. 1 (2012): 117–24. https://doi.org/10.1021/jz201525m.
55. Perdew, John P., Adrienn Ruzsinszky, Jianmin Tao, Viktor N. Staroverov, Gustavo E. Scuseria, and Gábor I. Csonka. "Prescription for the Design and Selection of Density Functional Approximations: More Constraint Satisfaction with Fewer Fits." *The Journal of Chemical Physics* 123, no. 6 (2005): 062201. https://doi.org/10.1063/1.1904565.
56. Becke, Axel D. "Density-functional Thermochemistry. III. The Role of Exact Exchange." *The Journal of Chemical Physics* 98, no. 7 (1993): 5648–52. https://doi.org/10.1063/1.464913.
57. Grimme, Stefan, and Frank Neese. "Double-Hybrid Density Functional Theory for Excited Electronic States of Molecules." *The Journal of Chemical Physics* 127, no. 15 (2007): 154116. https://doi.org/10.1063/1.2772854.
58. Tsipis, Athanassios C., A. Guy Orpen, and Jeremy N. Harvey. "Substituent Effects and the Mechanism of Alkene Metathesis Catalyzed by Ruthenium Dichloride Catalysts." *Dalton Trans.*, no. 17 (2005): 2849–58. https://doi.org/10.1039/B506929G.
59. Zhao, Yan, Nathan E. Schultz, and Donald G. Truhlar. "Design of Density Functionals by Combining the Method of Constraint Satisfaction with Parametrization for Thermochemistry, Thermochemical Kinetics, and Noncovalent Interactions." *Journal of Chemical Theory and Computation* 2, no. 2 (2006): 364–82. https://doi.org/10.1021/ct0502763.

60. Lundberg, Marcus, and Per E. M. Siegbahn. “Quantifying the Effects of the Self-Interaction Error in DFT: When Do the Delocalized States Appear?” *The Journal of Chemical Physics* 122, no. 22 (2005): 224103. https://doi.org/10.1063/1.1926277.

61. Amusia, M. Ya, and K. T. Taylor. *Atomic Photoeffect*. Physics of Atoms and Molecules. New York: Plenum Press, 1990.

62. Jana, Subrata, Szymon Śmiga, Lucian A. Constantin, and Prasanjit Samal. “Generalizing Double-Hybrid Density Functionals: Impact of Higher-Order Perturbation Terms.” *Journal of Chemical Theory and Computation* 16, no. 12 (2020): 7413–30. https://doi.org/10.1021/acs.jctc.0c00823.

63. Møller, Chr., and M. S. Plesset. “Note on an Approximation Treatment for Many-Electron Systems.” *Phys. Rev.* 46, no. 7 (October 1934): 618–22. https://doi.org/10.1103/PhysRev.46.618.

64. Peng, Chunyang, Philippe Y. Ayala, H. Bernhard Schlegel, and Michael J. Frisch. “Using Redundant Internal Coordinates to Optimize Equilibrium Geometries and Transition States.” *Journal of Computational Chemistry* 17, no. 1 (1996): 49–56. https://doi.org/10.1002/(SICI)1096-987X(19960115)17:1<49::AID-JCC5>3.0.CO;2-0.

65. Gaussian 16, Revision C.01, Frisch, M. J.; Trucks, G. W.; Schlegel, H. B.; Scuseria, G. E.; Robb, M. A.; Cheeseman, J. R.; Scalmani, G.; Barone, V.; Petersson, G. A.; Nakatsuji, H.; Li, X.; Caricato, M.; Marenich, A. V.; Bloino, J.; Janesko, B. G.; Gomperts, R.; Mennucci, B.; Hratchian, H. P.; Ortiz, J. V.; Izmaylov, A. F.; Sonnenberg, J. L.; Williams-Young, D.; Ding, F.; Lipparini, F.; Egidi, F.; Goings, J.; Peng, B.; Petrone, A.; Henderson, T.; Ranasinghe, D.; Zakrzewski, V. G.; Gao, J.; Rega, N.; Zheng, G.; Liang, W.; Hada, M.; Ehara, M.; Toyota, K.; Fukuda, R.; Hasegawa, J.; Ishida, M.; Nakajima, T.; Honda, Y.;

Kitao, O.; Nakai, H.; Vreven, T.; Throssell, K.; Montgomery, J. A., Jr.; Peralta, J. E.; Ogliaro, F.; Bearpark, M. J.; Heyd, J. J.; Brothers, E. N.; Kudin, K. N.; Staroverov, V. N.; Keith, T. A.; Kobayashi, R.; Normand, J.; Raghavachari, K.; Rendell, A. P.; Burant, J. C.; Iyengar, S. S.; Tomasi, J.; Cossi, M.; Millam, J. M.; Klene, M.; Adamo, C.; Cammi, R.; Ochterski, J. W.; Martin, R. L.; Morokuma, K.; Farkas, O.; Foresman, J. B.; Fox, D. J. Gaussian, Inc., Wallingford CT, 2016.

66. Ehlers, A. W., M. Böhme, S. Dapprich, A. Gobbi, A. Höllwarth, V. Jonas, K. F. Köhler, R. Stegmann, A. Veldkamp, and G. Frenking. "A Set of F-Polarization Functions for Pseudo-Potential Basis Sets of the Transition Metals Sc□Cu, Y□Ag and La□Au." *Chemical Physics Letters* 208, no. 1 (1993): 111–14. https://doi.org/10.1016/0009-2614(93)80086-5.

67. Höllwarth, A., M. Böhme, S. Dapprich, A. W. Ehlers, A. Gobbi, V. Jonas, K. F. Köhler, R. Stegmann, A. Veldkamp, and G. Frenking. "A Set of D-Polarization Functions for Pseudo-Potential Basis Sets of the Main Group Elements Al□Bi and f-Type Polarization Functions for Zn, Cd, Hg." *Chemical Physics Letters* 208, no. 3 (1993): 237–40. https://doi.org/10.1016/0009-2614(93)89068-S.

68. Hehre, W. J., R. Ditchfield, and J. A. Pople. "Self—Consistent Molecular Orbital Methods. XII. Further Extensions of Gaussian—Type Basis Sets for Use in Molecular Orbital Studies of Organic Molecules." *The Journal of Chemical Physics* 56, no. 5 (1972): 2257–61. https://doi.org/10.1063/1.1677527.

69. Marenich, Aleksandr V., Christopher J. Cramer, and Donald G. Truhlar. "Universal Solvation Model Based on Solute Electron Density and on a Continuum Model of the Solvent Defined by the Bulk Dielectric Constant and Atomic Surface Tensions." *The Journal of Physical Chemistry B* 113, no. 18 (2009): 6378–96. https://doi.org/10.1021/jp810292n.

70. (a) McLean, A. D., and G. S. Chandler. “Contracted Gaussian Basis Sets for Molecular Calculations. I. Second Row Atoms, Z=11–18.” *The Journal of Chemical Physics* 72, no. 10 (1980): 5639–48. https://doi.org/10.1063/1.438980 (b) Krishnan, R., J. S. Binkley, R. Seeger, and J. A. Pople. “Self-consistent Molecular Orbital Methods. XX. A Basis Set for Correlated Wave Functions.” *The Journal of Chemical Physics* 72, no. 1 (1980): 650–54. https://doi.org/10.1063/1.438955.

71. (a) Ribeiro, Raphael F., Aleksandr V. Marenich, Christopher J. Cramer, and Donald G. Truhlar. “Use of Solution-Phase Vibrational Frequencies in Continuum Models for the Free Energy of Solvation.” *The Journal of Physical Chemistry B* 115, no. 49 (2011): 14556–62. https://doi.org/10.1021/jp205508z. (b) Zhao, Yan, and Donald G. Truhlar. “Computational Characterization and Modeling of Buckyball Tweezers: Density Functional Study of Concave–Convex Π···π Interactions.” *Phys. Chem. Chem. Phys.* 10, no. 19 (2008): 2813–18. https://doi.org/10.1039/B717744E.

72. Pettersen, Eric F., Thomas D. Goddard, Conrad C. Huang, Gregory S. Couch, Daniel M. Greenblatt, Elaine C. Meng, and Thomas E. Ferrin. “UCSF Chimera—A Visualization System for Exploratory Research and Analysis.” *Journal of Computational Chemistry* 25, no. 13 (2004): 1605–12. https://doi.org/10.1002/jcc.20084.

73. Kruse, Holger, Lars Goerigk, and Stefan Grimme. “Why the Standard B3LYP/6-31G* Model Chemistry Should Not Be Used in DFT Calculations of Molecular Thermochemistry: Understanding and Correcting the Problem.” *The Journal of Organic Chemistry* 77, no. 23 (2012): 10824–34. https://doi.org/10.1021/jo302156p.

74. Chéron, Nicolas, Denis Jacquemin, and Paul Fleurat-Lessard. “A Qualitative Failure of B3LYP for Textbook Organic Reactions.” *Phys. Chem. Chem. Phys.* 14, no. 19 (2012): 7170–75. https://doi.org/10.1039/C2CP40438A.

75. Hammond, George S. “A Correlation of Reaction Rates.” *Journal of the American Chemical Society* 77, no. 2 (1955): 334–38. https://doi.org/10.1021/ja01607a027.

BIOGRAPHICAL SKETCH

Dominique Celine Gallegos was born in McAllen, TX on January 28th, 1997. While growing up, she always had a fondness for science. She graduated from James 'Nikki' Rowe High School in 2015. She attended the University of Texas at Austin (UT) where she received a Bachelor of Science and Arts Degree in Chemistry with a certificate in Forensic Science in 2019. That same year, Dominique continued her education at the University of Texas at Rio Grande Valley (UTRGV) to obtain her master's degree in Chemistry. Dominique worked as a Graduate Teaching Assistant for the Chemistry department during this time, where she learned to teach a multitude of courses and laboratories including General Chemistry, Organic Chemistry, Analytical Chemistry, and Physical Chemistry. She graduated with her M.S. Chemistry Degree from UTRGV on May 6th, 2021.

Permanent Mailing address: 3104 Kiwi Ave. McAllen, TX, 78541

Author can be reached at: dominique.gallegos28@gmail.com